Title

Differential Vulnerability of CA1 versus CA3 Pyramidal Neurons After Ischemia: Possible Relationship to Sources of Zn2+ Accumulation and Its Entry into and Prolonged Effects on Mitochondria

Journal

Journal of Neuroscience, 37(3)

ISSN

0270-6474

Authors

Medvedeva, Yuliya V
Ji, Sung G
Yin, Hong Z
et al.

Publication Date

2017-01-18

DOI

10.1523/jneurosci.3270-16.2016

Peer reviewed

The Journal of Neuroscience

http://jneurosci.msubmit.net

JN-RM-3270-16R1

Differential vulnerability of CA1 vs CA3 pyramidal neurons after ischemia: possible relationship to sources of Zn2+ accumulation and its entry into and prolonged effects on mitochondria

John Weiss, University of California Irvine
Yuliya Medvedeva, University of Iowa
Sung Ji, University of California, Irvine
Hong Z. Yin, University of California Irvine

Commercial Interest:

Section: Neurobiology of Disease

Differential vulnerability of CA1 vs CA3 pyramidal neurons after ischemia: possible relationship to sources of Zn^{2+} accumulation and its entry into and prolonged effects on mitochondria

Yuliya V. Medvedeva[1], Sunggoan Ji[2], Hong Z. Yin[1] and John H. Weiss[1]

Departments of [1]Neurology & [2]Anatomy and Neurobiology
University of California Irvine,
Irvine, CA 9269

Corresponding Author:
J. H. Weiss, MD, Ph.D.
Department of Neurology
University of California, Irvine
Irvine, CA 92697-4299, USA
Ph: (949) 824-6774
Fax: (949) 824-1668
Email: jweiss@uci.edu

Abbreviated Title: ***Zn^{2+} and ischemic injury to CA1 and CA3 neurons***

Number of pages: 32
Number of figures: 8
Number of tables: 0

Number of words: Abstract - **249**
Introduction - **641**
Discussion - 1479

Keywords: hippocampal slice, mitochondria, zinc, calcium, Ca^{2+}, ischemia, Ruthenium Red, mitochondrial Ca^{2+} uniporter, oxygen glucose deprivation

Acknowledgements: Supported by NIH grants NS065219 and NS096987 (J.H.W.). We thank Edward Sharman for editorial assistance and helpful discussions. The authors declare no competing financial interests.

Abstract: Excitotoxic mechanisms contribute to the degeneration of hippocampal pyramidal neurons after recurrent seizures and brain ischemia. However, susceptibility differs, with CA1 neurons preferentially degenerating after global ischemia, and CA3 neurons after limbic seizures. Whereas most studies address contributions of excitotoxic Ca^{2+} entry, it is apparent that Zn^{2+} also contributes, reflecting accumulation in neurons either **after synaptic release** and entry through post-synaptic channels or upon mobilization from intracellular Zn^{2+} binding proteins like metallothionein-III (**MT-III**). **Using mouse hippocampal slices** to study acute oxygen glucose deprivation (**OGD**) triggered neurodegeneration, we find evidence for early contributions of excitotoxic Ca^{2+} and Zn^{2+} accumulation in both CA1 and CA3, as indicated by the ability of Zn^{2+} chelators or Ca^{2+} entry blockers to delay pyramidal neuronal death in both regions. However, using knockout animals (of MT-III and vesicular Zn^{2+} transporter, **ZnT3**) and channel blockers revealed substantial differences in relevant Zn^{2+} sources, with critical contributions of pre-synaptic release and its permeation through Ca^{2+} (and Zn^{2+}) permeable AMPA channels in CA3, and Zn^{2+} mobilization from MT-III predominating in CA1. To assess consequences of the intracellular Zn^{2+} accumulation, we employed OGD exposures slightly shorter than those causing acute neuronal death; under these conditions, cytosolic Zn^{2+} rises persisted for 10-30 min after OGD, followed by recovery over ~40-60 min. Furthermore, the recovery appeared to be accompanied by mitochondrial Zn^{2+} accumulation (via the mitochondrial Ca^{2+} uniporter, **MCU**) in CA1 but not in CA3 neurons, that was markedly diminished in MT-III knockouts, suggesting that it depended upon Zn^{2+} mobilization from this protein.

Significance Statement: The basis for the differential vulnerabilities of CA1 vs CA3 pyramidal neurons is unclear. Present studies of events during and after acute OGD highlight a possible important difference, with rapid synaptic entry of Ca^{2+} and Zn^{2+} contributing more in CA3, but with delayed and long lasting accumulation of Zn^{2+} within mitochondria occurring in CA1 but not CA3 pyramidal neurons. These data may be consistent with observations of prominent mitochondrial dysfunction as a critical early event in the delayed degeneration of CA1 neurons after ischemia, and support a hypothesis that mitochondrial Zn^{2+} accumulation in the early reperfusion period may be a critical and targetable upstream event in the injury cascade.

Introduction

Hippocampal pyramidal neurons (HPNs) of the CA1 and CA3 domains are highly vulnerable to injury in pathological conditions of prolonged or recurrent seizures, or after brain ischemia. However, their patterns of vulnerability differ, likely reflecting differences in events leading to their degeneration. CA3 neurons are preferentially lost in response to limbic seizures occurring after kainic acid injection into the amygdala (Ben-Ari et al., 1980a; Ben-Ari et al., 1980b; Tanaka et al., 1988). In contrast, delayed selective degeneration of CA1 neurons is conspicuous after transient ischemia in humans (Zola-Morgan et al., 1986; Petito et al., 1987) and rodents (Kirino, 1982; Ordy et al., 1993; Sugawara et al., 1999).

Excitotoxic mechanisms, caused by excessive glutamate release, have long been considered important contributors to ischemic neurodegeneration. Most studies have focused upon the role of rapid Ca^{2+} entry through NMDA type glutamate receptors. Indeed, glutamate triggered injury to cultured neurons is Ca^{2+} dependent (Choi, 1987), and delayed sharp Ca^{2+} rises, occurring after the end of the glutamate exposures, are indicative of cell death (Rothman and Olney, 1986; Siesjo, 1988; Randall and Thayer, 1992). However, despite intense early interest, clinical efficacy of glutamate antagonists has been limited.

Further studies have highlighted contributions of another divalent cation, Zn^{2+}, which is present in the brain at high levels, accumulates in hippocampal pyramidal neurons after ischemia or prolonged seizures, and has been implicated in ischemic neurodegeneration (Frederickson et al., 1989; Tonder et al., 1990; Koh et al., 1996; Yin et al., 2002; Calderone et al., 2004). **It is apparent that there are two distinct sources of the Zn^{2+} that accumulates in neurons after ischemia or prolonged seizures. One comprises presynaptic vesicular Zn^{2+} that is released and enters the postsynaptic neurons ("translocation"), likely in large part through highly Ca^{2+} permeable AMPA (Ca-AMPA) channels (which are also highly Zn^{2+} permeable) (Yin et al., 2002; Calderone et al., 2004; Noh et al., 2005). In addition, Zn^{2+} can be released from cytosolic buffering proteins like metallothioneins (MTs) already present in the neurons (Aizenman et al., 2000; Lee et al., 2000; Lee et al., 2003).**

Early effects of ischemia can be studied in brain slices subjected to oxygen–glucose deprivation (**OGD**), a procedure that mimics some aspects of stroke. Hippocampal slice models have revealed Zn^{2+} rises to

begin shortly after OGD onset and to contribute to subsequent injury (Yin et al., 2002; Wei et al., 2004; Stork and Li, 2006). To discriminate early effects of Zn^{2+} from those of Ca^{2+}, we simultaneously tracked these ions in CA1 pyramidal neurons in acute hippocampal slices subjected to OGD. **We found Zn^{2+} rises to precede and contribute to the induction of the terminal sharp Ca^{2+} rises** ("**Ca deregulations**"), which were causatively linked to a loss of membrane integrity (Medvedeva et al., 2009). The early Zn^{2+} rises resulted in mitochondrial accumulation (via the mitochondrial Ca^{2+} uniporter, **MCU**), contributing to their dysfunction and reactive oxygen species (**ROS**) generation (Medvedeva and Weiss, 2014).

Present slice studies show that Zn^{2+} clearly contributes to acute OGD induced injury in both CA1 and CA3 neurons, and further seek to examine differences in early events between these neuronal populations that may bear upon their differential vulnerabilities. Our findings suggest that pre-synaptic Zn^{2+} release and entry through Ca-AMPA channels dominates in CA3, whereas Zn^{2+} mobilization from MT-III is of greater importance in CA1. Furthermore, when we carried out OGD exposures just short of those that induce acute cell death, there was substantial ongoing Zn^{2+} accumulation in mitochondria of CA1 (but not in CA3) neurons persisting for at least ~30 min after OGD. These findings support the hypothesis that delayed mitochondrial Zn^{2+} accumulation might be a critical trigger of mitochondrial dysfunction and selective degeneration of CA1 pyramidal neurons after transient ischemia. As the Zn^{2+} accumulation progresses during the early post ischemic period, delivery of appropriate therapeutics during this period may have potential to provide substantial benefit.

Materials and Methods

Animals. All procedures were performed according to a protocol approved by University of California Irvine Animal Care and Use Committee. Efforts were made to minimize animal suffering and number of mice used. Three strains of mice **of either sex** were used for experiments: wild type mice 129S6/SvEvTac (Taconic Biosciences), **mice lacking metallothionein III (004649 - 129S7-$Mt3^{tm1Rpa}$/J,** Jackson Laboratory) and **mice lacking vesicular Zn^{2+} transporter (005064 - B6;129-$Slc30a3^{tm1Rpa}$/J,**

Jackson Laboratory). The strain of origin for both of these knockouts is **129S7/SvEvBrd-Hprt<+>**. We have characterized the occurrence of OGD induced Zn^{2+} rises and Ca^{2+} deregulation in each of these knockout strains, and find that Zn^{2+} rises precede Ca^{2+} deregulation in both CA1 and CA3 in both of these strains much as in the WT mice, with no evidence for any generalized differences in viability; the small deviations noted from WT occur in opposite directions in CA1 and CA3 neurons, and, in all cases are explainable based upon prior studies and expectations of the roles of the deleted peptides (MT-III or ZnT3; data not shown). However, despite the reasonable match between these strains, we cannot rule out the possibility of functionally significant differences and consequently only make statistical comparisons between responses within the same strain.

Preparation of acute hippocampal slices. Hippocampal slices were prepared from ~4 week old mice as previously described (Medvedeva, 2009). Mice were deeply anesthetized with isoflurane and decapitated, and the brains rapidly removed and placed in ice-cold preparation solution containing (in mM): Sucrose 220, KCl 3, NaH_2PO_4 1.25, $MgSO_4$ 6, $NaHCO_3$ 26, $CaCl_2$ 0.2, Glucose 10 and ketamine 0.42 (pH 7.35, 310 mOsm, equilibrated with 95 % O_2 / 5% CO_2). Hippocampal slices (300 μm) were cut with a vibratome (Leica VT1200), and placed in artificial CSF (ACSF) containing (in mM): NaCl 126, KCl 3, NaH_2PO_4 1.25, $MgSO_4$ 1, $NaHCO_3$ 26, $CaCl_2$ 2, Glucose 10 (pH 7.35, 310 mOsm, adjusted with sucrose and equilibrated with 95% O_2 / 5% CO_2). After equilibration for 1 hour at 34±0.5ºC, slices were kept at room temperature (20-23ºC) in oxygenated ACSF for at least 1 h before use.

Loading individual hippocampal neurons with fluorescent indicators. For recordings, slices were placed in a flow-through chamber (RC-27L chamber with plastic slice anchor, Warner instruments) mounted on the stage of an upright microscope (BX51WI Olympus, Japan) and perfused with oxygenated ACSF at 2 ml/min. Experiments were performed at 32±0.5ºC. Fura-FF, FluoZin-3 or AlexaFluor-488 were dissolved in pipette solution (containing, in mM: 125 KGluconate, 10 KCl, 3 Mg-ATP, 1 $MgCl_2$, 10 HEPES, pH 7.25 with KOH, 290 mOsm with sucrose) at concentrations of 1, 1, and 0.25 mM respectively, and 1 μl placed in the tip of a micropipette (5-7 MΩ, borosilicate glass with filament), prior to backfilling with pipette solution. Neurons were loaded with fluorescent indicators via patch pipettes by holding them in

150 the whole-cell configuration at -60 mV for 5 min, as previously described (Medvedeva et al., 2009).
151 During pipette withdrawal, cells were monitored to assess membrane leakage and Ca^{2+} levels; intact cells
152 were left to recover for 20 min before starting experiment.
153 ***Fluorescent measurements.*** For simultaneous measurements of intracellular Ca^{2+} and Zn^{2+} dynamics,
154 cells were co-loaded with a low affinity Ca^{2+} indicator (Fura-FF, K_d~5.5 μM) and a high affinity Zn^{2+}
155 indicator FluoZin-3 (K_d~15 nM). To assess changes in membrane integrity, the ion insensitive fluorescent
156 compound, AlexaFluor-488 was co-loaded with Fura-FF. Fluorescence was alternately excited at 340(20),
157 380(20) 482(20) nm via a 40x water-immersion objective, using a Xenon light source (Sutter
158 Instruments), and emitted fluorescence collected at 532 (40) nm using a cooled CCD camera
159 (Hamamatsu, Japan) (All filters are bandpass with bandwidths indicated in parentheses.) Images were
160 acquired every 15 or 30 sec, background subtracted and analyzed using METAFLUOR 7.1 software
161 (Universal Imaging). Changes in Ca^{2+} values are presented as the ratio of background subtracted Fura-FF
162 emission intensities upon excitation at 340 and 380 nm ("340/380 ratio"), FluoZin-3 fluorescence changes
163 are presented as $\Delta F/F_0=(F-F_0)/F_0$, and AlexaFluor-488 fluorescence changes as F/F_0, where F is the
164 current fluorescence intensity and F_0 is the average background-subtracted baseline fluorescence during
165 the 10 min prior to OGD.
166 To assess changes in mitochondrial potential ($\Delta\Psi_m$) slices were bulk loaded with the $\Delta\Psi_m$ sensitive
167 indicator, Rhodamine 123 (Rhod123, 26 μM, 30 min, 20-23 ºC). Rhod123 is positively charged and
168 accumulates in negatively charged mitochondria where its fluorescence is quenched. Upon mitochondrial
169 depolarization **it is released into the cytoplasm causing an increase in fluorescence** (Duchen et al.,
170 2003). Rhod123 was excited at 540(25) nm and emitted fluorescence collected at 605(55) nm. Images
171 were acquired every 15 s, and data presented as $\Delta F/F_0=(F-F_0)/F_0$ where F is a current fluorescence
172 intensity and F_0 is the fluorescence intensity in the resting slice. Regions of interest were monitored in the
173 CA1 or CA3 pyramidal cell layers.
174 ***Oxygen-glucose deprivation (OGD) in slices.*** To simulate hypoxic-hypoglycemic conditions, ACSF was
175 changed to identical solution lacking glucose and bubbled with 95% N_2 / 5% CO_2. In studies examining

acute OGD induced neurodegeneration, OGD was continued for at least 15 min, and maintained through the time of the terminal Ca^{2+} deregulation. For sublethal OGD exposures, OGD was terminated (by restoration of oxygenated ACSF) ~1 min after start of the Zn^{2+} rise in experiments where Zn^{2+} was measured (typically occurring from 6-9 min), or, for the Rhod123 (Fig. 5) and confocal imaging (Fig. 7) studies, after 8.5-9 min as indicated.

MK-801 (10 μM), Nimodipine (10 μM), 1-Naphthyl acetyl spermine (NASPM, 100 μM) and N,N,N',N'-tetrakis(2-pyridylmethyl)ethane-1,2-diamine (TPEN, 40 μM) were applied 10 min prior to and during OGD. Ruthenium Red (10 μM) and carbonyl cyanide-4-(trifluoromethoxy)phenylhydrazone (FCCP, 2 μM) were applied after the termination of OGD as indicated.

Antibody labeling and confocal microscopy. Hippocampal slices (300 μm) were subjected to OGD as described for 8.5 min, "perfused" in ACSF at 32ºC for 1 hr, and immediately fixed with 4% paraformaldehyde. **Thin (30 μm) sections were cut using a microtome cryostat** (ThermoFisher Scientific, Waltham, MA) and stained with primary antibodies against the mitochondrial outer membrane protein TOM20 (1:200, Santa Cruz Biotechnology, Santa Cruz, CA) and secondary anti-rabbit fluorescent antibodies (1:200, DyLight™ 488, Jackson ImmunoResearch, West Grove, PA) . The sections were imaged using an inverted stage Nikon Eclipse Ti chassis microscope with Yokogawa CSUX spinning disk head, a 100x (1.49 n.a.) objective, and images acquired using a Hamamatsu electromultiplying CCD camera. Excitation (488 nm) was via a Coherent Sapphire laser source synchronized with the camera, emission monitored with a 525 (50) nm filter, and images were acquired using MIcroManager ImageAcquisition sofrware (v1.4.16). **Brightfield images** were obtained using the same objective at the same z-axis position immediately after acquiring fluorescent image.

For analysis of mitochondria size and shape (using ImageJ software) we selected large neurons in the pyramidal cell layer. To control for differing behavior of mitochondria between distinct cell types and cellular compartments, we chose to focus our studies on mitochondria surrounding the prominent nucleii of pyramidal neurons, and selected fields for analysis in which mitochondria were clearly evident in perinuclear regions, in the plane of sharp focus. Images were adjusted to provide optimal discrimination

of their apparent edges from background. In the perinuclear regions, mitochondria are aligned with their long axes parallel to the nuclear membrane. Nuclear regions in which clearly demarcated mitochondria were evident were cropped from images and saved with a code name for blinded measurements, and measures (of long axes, parallel to, and short axes, perpendicular to nuclear membranes) obtained on all clearly demarcated mitochondria adjacent to and surrounding the nuclear circumference. Mean parameters were determined for mitochondria within each cell, the cell values were averaged to determine the mean paramaters within each independent slice, and presented values are means from 3-5 slices for each condition.

Reagents: Fura-FF, FluorZin-3, Rhodamine 123 and AlexaFluor-488 hydrazide were obtained from Invitrogen (Carlsbad, CA). MK-801 was obtained from Abcam (Cambridge, UK), N,N,N',N'-Tetrakis(2-pyridylmethyl)ethylenediamine (TPEN), Ruthenium Red and ketamine were obtained from Sigma (St. Louis, MO). Nimodipine was obtained from Miles Inc. (West Haven, CT). 1-Naphthyl acetyl spermine (NASPM) was obtained from Tocris Bioscience (Bristol, UK). TOM20 antibodies were obtained from Santa Cruz Biotechnology (Santa Cruz, CA; Cat # sc-11415, ***RRID*:AB_2207533**) and DyLight™ 488 antibodies were obtained from Jackson ImmunoResearch (West Grove, PA; Cat # 211-482-171). All other reagents were purchased from Fisher Scientific.

Statistics and data analysis. The onset times of OGD-induced Zn^{2+} rises and of Ca^{2+} deregulations were determined by finding intersections between the extrapolated baselines, with lines fitting the first substantial FluoZin-3 fluorescence increases or Fura-FF ratio increases, as previously described (Medvedeva et al., 2009). Differences between sets of data were assessed using two sample t-tests (Origin 9.1). In some studies we sought to determine whether the degree of protection provided by an intervention (assessed as the mean interval between the time of Ca^{2+} deregulation in control and treatment groups) or the interval between the Zn^{2+} rise and the Ca^{2+} deregulation differed between CA1 and CA3 neurons. For these assessments we used the ANOVA linear contrast test (STATA software). All comparisons reflect sets of data substantially interleaved in time, and were based on 5 –10 slices from ≥5

227 animals each condition (numbers of cells and slices are indicated for each experiment), and all values are
228 presented as means±SEM.

229 **Results**

230 ***Ca^{2+} and Zn^{2+} contribute to OGD induced degeneration of both CA3 and CA1 pyramidal neurons***

231 In recent studies (Medvedeva et al., 2009; Medvedeva and Weiss, 2014), we examined Ca^{2+} and Zn^{2+}
232 changes in hippocampal CA1 pyramidal neurons during acute OGD, and their respective contributions to
233 neuronal injury. When the slices were subjected to OGD, we found that cytosolic Zn^{2+} rises began within
234 several minutes and preceded very high cytosolic Ca^{2+} rises (termed "Ca^{2+} deregulation" events), which
235 were terminal events, as they were accompanied by a loss of membrane integrity. These Ca^{2+}
236 deregulations were delayed by addition of the high affinity Zn^{2+} chelator, N,N,N′,N′-Tetrakis(2-
237 pyridylmethyl)ethylenediamine (TPEN), indicating a contribution of the Zn^{2+} to the cell death cascade.

238 Since there are likely to be therapeutically significant differences in the sequence of events linking
239 ischemia to degeneration of CA1 vs CA3 neurons, we employed the same paradigm to examine
240 contribution of Zn^{2+} and Ca^{2+} in acute ischemic degeneration of CA3 neurons. As in our prior studies,
241 single neurons in acute slices were co-loaded with membrane impermeable forms of the high affinity Zn^{2+}
242 indicator FluoZin-3 (K_d~ 15 nM) and a low affinity ratiometric Ca^{2+} indicator (Fura-FF; K_d ~ 5.5 μM)
243 via a patch pipette, and the slices subjected to OGD as described [(Medvedeva et al., 2009; Medvedeva
244 and Weiss, 2014); see Materials and Methods], while monitoring changes in cytosolic Zn^{2+} (as $\Delta F/F_o$) and
245 Ca^{2+} (as 340/380 ratio). We found that as in CA1, Zn^{2+} rises preceded Ca^{2+} deregulation events in CA3
246 (**Fig. 1A,B**).

247 To confirm that the Ca^{2+} deregulations were terminal events in CA3, other neurons were co-loaded
248 with the low affinity Ca^{2+} indicator (Fura-FF) along with the ion insensitive fluorescent compound,
249 AlexaFluor-488. As in CA1 (Medvedeva et al., 2009), Ca^{2+} deregulation was always accompanied by the
250 onset of a dramatic loss of AlexaFluor-488 fluorescence in the absence of any recovery of the cytosolic
251 Ca^{2+}, indicating a terminal loss of membrane integrity (Randall and Thayer, 1992; Vander Jagt et al.,
252 2008) (**Fig. 1A**). Furthermore, the Ca^{2+} deregulation in CA3 pyramidal neurons was delayed by Zn^{2+}

chelation (with TPEN, 40 μM) to a similar degree as in CA1 (**Fig. 1C**), indicating that Zn^{2+} contributes to the onset of this terminal event in both subfields.

"Excitotoxicity" contributes to OGD induced degeneration in both CA3 and CA1 pyramidal neurons

Most studies of acute excitotoxicity have focused upon the contribution of rapid Ca^{2+} entry through highly Ca^{2+} permeable NMDA receptor-gated channels. Ca^{2+} can also enter depolarized neurons via voltage gated Ca^{2+} channels (**VGCC**). To assess the contribution of these Ca^{2+} entry routes to OGD induced degeneration, we tested effects of the NMDA blocker MK-801 alone, or in the additional presence of the VGCC blocker nimodipine (each at 10 μM; added 10 min before start of OGD). Each of these treatments delayed Ca^{2+} deregulation in both CA3 and CA1 neurons. Interestingly, each of these treatments provided significantly greater protection in CA3 than in CA1, suggesting a greater acute excitotoxic contribution to ischemic injury in CA3 (**Fig. 2**), possibly consistent with the greater susceptibility of CA3 neurons to recurrent limbic seizures.

Critical contribution of Zn^{2+} entry through Ca-AMPA to acute OGD injury in CA3

AMPA-type glutamate receptors, which mediate most rapid excitatory neurotransmission, are tetramers, comprised of combinations of four subunits (GluA1-4). Whereas most AMPA channels are Ca^{2+} impermeable, those lacking the GluA2 subunit are Ca^{2+} permeable (Ca-AMPA channels) (Hollmann et al., 1991; Verdoorn et al., 1991). While it was originally thought that pyramidal neurons express few Ca-AMPA channels, it later became apparent that they are present at variable levels on many pyramidal neurons, and may be preferentially found in dendritic membranes adjacent to sites of presynaptic glutamate release (Lerma et al., 1994; Yin et al., 1999; Ogoshi and Weiss, 2003). In addition to being Ca^{2+} permeable, these channels, unlike NMDA channels, are also highly permeable to Zn^{2+} (Yin and Weiss, 1995; Sensi et al., 1999; Jia et al., 2002) and are likely important routes for entry of synaptically released Zn^{2+} into post-synaptic neurons (Yin et al., 2002; Noh et al., 2005).

To block these channels we used the selective Ca-AMPA channel blocker, 1-naphthyl acetyl spermine (NASPM), a synthetic analog of joro spider toxin (Koike et al., 1997; Yin et al., 2002; Noh et al., 2005). Whereas NASPM (100 μM; added 10 min before start of OGD) significantly delayed Ca^{2+} deregulation in CA3 pyramidal neurons, it had no effect on the time of Ca^{2+} deregulation in CA1 (**Fig. 3A**). Yet, as Ca-AMPA channels are permeable to Ca^{2+} as well as Zn^{2+}, we wondered whether inhibition of Ca^{2+} or Zn^{2+} entry was the more important factor in the protective effects of NASPM in CA3. To determine whether the protection provided by NASPM was due to specific blockade of Zn^{2+} entry through Ca-AMPA channels, we made use of the mice lacking the vesicular Zn^{2+} transporter, ZnT3, which are completely lacking in presynaptic vesicular Zn^{2+} (Cole et al., 1999). In slices prepared from ZnT3 knockout mice (**ZnT3 KOs**), OGD still triggered Zn^{2+} rises and subsequent Ca^{2+} deregulation (not shown), much as we observed in WT's. However, the previously observed protective effects of NASPM, as well as of the Zn^{2+} chelator, TPEN were entirely absent in CA3 neurons of the ZnT3 KOs, strongly arguing that the beneficial effect of NASPM in slices prepared from WT mice was largely due to antagonism of the passage of synaptically released Zn^{2+} through Ca-AMPA channels (**Fig. 3B**). In contrast to the absence of protective effect of TPEN in ZnT3 KOs in CA3, TPEN was still substantially protective in CA1, suggesting that the sources of the Zn^{2+} that contribute to acute OGD induced injury differ between these hippocampal subzones.

Zn^{2+} mobilization from MT-III contributes to OGD induced degeneration of CA1 neurons

Observations that Zn^{2+} is stored in pre-synaptic vesicles, undergoes activity dependent release, and that loss of pre-synaptic Zn^{2+} occurs concomitantly with Zn^{2+} accumulation in degenerating post-synaptic neurons after ischemia or prolonged seizures led to the expectation that Zn^{2+} "translocation" accounted for the injurious Zn^{2+} accumulation noted to occur in these conditions (Frederickson, 1989; Frederickson et al., 1989; Tonder et al., 1990; Koh et al., 1996). However, using ZnT3 KO mice, the surprising observation was made that, rather than the expected decreases, Zn^{2+} accumulation and damage to CA1 pyramidal neurons were actually increased (Lee et al., 2000). A subsequent study using MT-III KOs as

well as double MT-III/ZnT3 KOs suggested that much of the delayed Zn^{2+} accumulation seen after prolonged seizures in CA1 pyramidal neurons of ZnT-3 KOs was due to Zn^{2+} mobilization from MT-III (Lee et al., 2003).

To assess contributions of MT-III bound Zn^{2+} to acute OGD induced degeneration, we used slices from MT-III KO mice. In these slices, OGD still triggered Zn^{2+} rises and subsequent Ca^{2+} deregulation (not shown), much as in both WT's and ZnT3 KOs. Whereas Zn^{2+} chelation with TPEN delayed Ca^{2+} deregulation in CA3 pyramidal neurons (much as in WT's; see Fig. 1), protective effects of TPEN were absent in CA1 neurons of the MT-III KOs (**Fig. 4A**). This strongly suggests that the Zn^{2+} contribution to acute OGD induced degeneration of CA1 (but not CA3) neurons is mediated largely by Zn^{2+} mobilization from MT-III. Despite the lack of substantial Zn^{2+} contribution to CA1 damage in these mice, Ca^{2+} entry blockers had protective effects in the MT-III KOs similar to those seen in WT slices in both CA1 and CA3 (**Fig. 4B**).

Protracted mitochondrial Zn^{2+} accumulation after sublethal OGD in CA1 but not in CA3 neurons

Whereas above studies highlighted distinct sources of the Zn^{2+} contributing to acute ischemic damage **in CA1 vs CA3 pyramidal neurons**, we next sought to examine clues to possible differences in targets or effects of the Zn^{2+} after the acute ischemic episode that might help to explain the differential vulnerabilities of CA1 and CA3 neurons in disease conditions. To this aim we carried out OGD of durations just short of those that induced acute Ca^{2+} deregulation and cell death, terminating OGD ~1 min after the onset of the cytosolic Zn^{2+} rise (which generally occurred between 6 and 9 minutes), and monitored cytosolic Ca^{2+} and Zn^{2+} for an additional 60-80 min. Under these conditions, cytosolic Zn^{2+} rises persisted for ~10-30 min after OGD, followed by recovery over ~40-60 min.

There are a number of reasons to suspect that mitochondria are important targets for deleterious effects of cytosolic Zn^{2+} accumulation (reviewed in the Discussion section, below). To assess mitochondrial Zn^{2+} accumulation after sublethal OGD exposures, we used the mitochondrial uncoupler, FCCP (2 μM, 5 min), which dissipates the proton gradient across the inner mitochondrial membrane, resulting in rapid

mitochondrial depolarization (**loss of $\Delta\Psi_m$**) and release of Zn^{2+} already present in mitochondria (Sensi et al., 2000; Sensi et al., 2002; Medvedeva et al., 2009; Clausen et al., 2013). **Application of FCCP 55-60 min after the end of the OGD episode resulted in a sharp cytosolic Zn^{2+} rise in CA1 neurons**, presumably due to the release of Zn^{2+} that had become sequestered in the mitochondria. However, Zn^{2+} responses to identical delayed FCCP treatments were almost absent in CA3 (**Fig. 5A,B,C**). One possible explanation for the absence of a cytosolic Zn^{2+} response to FCCP in CA3 could be that the mitochondria were already fully depolarized at that time and could not sequester Zn^{2+}. To test this, we used the $\Delta\Psi_m$ sensitive indicator Rhodamine 123 (**Rhod123**) to compare $\Delta\Psi_m$ between CA1 and CA3; an increase in fluorescence of this indicator is indicative of loss of $\Delta\Psi_m$. When added 50 min after the end of the OGD, FCCP triggered similar sharp increases in Rhod123 fluorescence (as $\Delta F/F_o$) in both CA1 and CA3 neurons, indicating a similar magnitude of $\Delta\Psi_m$ at this time point (**Fig. 5D,E**). Thus, the paucity of delayed mitochondrial Zn^{2+} uptake in CA3 does not appear to be explained by greater or more persistent loss of $\Delta\Psi_m$ in these neurons.

Zn^{2+} accumulation in CA1 mitochondria during "reperfusion" reflects mobilization from MT-III

We next used the MCU blocker Ruthenium Red (RR) (Moore, 1971; Medvedeva and Weiss, 2014) to elicit clues as to the time frame during which Zn^{2+} accumulates in the CA1 mitochondria (**Fig. 6**). When RR was applied for 15 min, starting 7-10 min after the end of the OGD (while cytosolic Zn^{2+} levels were still markedly elevated), application of FCCP 30 min later failed to elicit a Zn^{2+} rise (Fig. 6A), supporting the hypothesis that much of the Zn^{2+} may have entered the mitochondria during this period of elevated cytosolic Zn^{2+}. As a test of this idea, we also examined the effect of RR application at a later time point **(starting ~30-40 min after the end of the OGD)**, when cytosolic Zn^{2+} rises had largely recovered. With this treatment, subsequent FCCP (15 min after washout of the RR) did result in a large cytosolic Zn^{2+} rise (Fig. 6B). The simplest explanation for this observation is that the RR treatment at this later time point largely failed to prevent mitochondrial Zn^{2+} accumulation, as considerable Zn^{2+} had already entered the mitochondria, remaining sequestered within them at the time of the FCCP exposure. Notably however,

this delayed RR application caused a small increase in cytosolic Zn^{2+} (**Fig. 6B**, arrow, evident in all 6 cells examined) supporting the idea that free Zn^{2+} accumulation in the cytosol and its uptake into mitochondria was still ongoing at the indicated time (~40 min after OGD). Finally, to test the contribution of Zn^{2+} mobilization from MT-III to this delayed mitochondrial Zn^{2+} accumulation, we carried out an identical sublethal OGD exposure in slices from MT-III KOs. Interestingly, despite the absence of MT-III, we still saw cytosolic Zn^{2+} rises that persisted for a period of 10-20 min after the end of the OGD. However, upon delayed application of FCCP, cytosolic Zn^{2+} rises were considerably less than in WT (Fig. 6C).

Mitochondrial swelling after OGD in CA1 pyramidal neurons is attenuated by MCU blockade

Finally, to examine a possible consequence of the mitochondrial Zn^{2+} uptake in CA1 we employed confocal imaging to assess changes in mitochondrial morphology ~1 hour after sublethal OGD. Slices were exposed either to sham wash in oxygenated media (as control) or to a sublethal (~8.5 min) episode of OGD, either alone, or with RR applied 10 min after the end of the OGD for 15 min (**as in Fig. 6A, above**). One hour after OGD, slices were fixed, and immunolabeled with antibody for the mitochondrial outer membrane marker, TOM20. Slices were examined under confocal microscopy (1000x), and images obtained in the CA1 pyramidal layer (**Fig. 7A**). For quantitative assessment, images were adjusted (using Image J software) to optimally discriminate mitochondrial borders from background, and perinuclear regions cropped from images and coded for blinded measurement of mitochondrial lengths and widths (see Methods). We found that OGD caused a marked "rounding-up" of the mitochondria with substantial decreases in their mean lengths, increases in their widths, and decreased length / width (L/W) ratios. We further found that delayed application of RR attenuated this effect, yielding an intermediate L/W ratio (**Fig. 7B)**.

Discussion

Distinct "pools" contribute to injurious hippocampal Zn^{2+} accumulation in vivo

Despite high (>100 μM) levels of Zn^{2+} in the brain, under resting conditions it is almost all sequestered, such that free levels are very low (generally <1 nM) (Frederickson, 1989). One major site of Zn^{2+} sequestration is in synaptic vesicles, where it is stored via action of the vesicular Zn^{2+} transporter, ZnT3 (Cole et al., 1999), and undergoes activity dependent release (Assaf and Chung, 1984; Howell et al., 1984). Observations of Zn^{2+} accumulation in injured and degenerating neurons after prolonged seizures or ischemia (Frederickson et al., 1989; Tonder et al., 1990) led to the proposition that "Zn^{2+} translocation" across the synapse might contribute critically to the associated neurodegeneration. The link between Zn^{2+} accumulation and neurodegeneration was markedly strengthened by observations that the extracellular Zn^{2+} chelator, Ca-EDTA was highly protective in ischemia (Koh et al., 1996; Calderone et al., 2004). Studies of Zn^{2+} entry routes indicated permeation through VGCC, and, with particular rapidity, through Ca-AMPA channels (Weiss et al., 1993; Yin and Weiss, 1995; Sensi et al., 1999; Jia et al., 2002). Indeed, Zn^{2+} entry through Ca-AMPA channels appears to contribute to ischemic injury both acutely and at delayed time points after transient ischemia, after numbers of these channels have been upregulated (Yin et al., 2002; Noh et al., 2005).

The generation of ZnT3 KO mice provided a model to directly examine the specific contribution of synaptic Zn^{2+} release in neurodegeneration (Cole et al., 1999). Surprisingly, ZnT3 knockout actually increased the delayed Zn^{2+} accumulation and neuronal injury occurring after prolonged kainate seizures in CA1 neurons (while modestly decreasing them in CA3) (Lee et al., 2000). It subsequently became apparent that another important Zn^{2+} pool is that which is bound to Zn^{2+} buffering proteins like metallothioneins (MT-III being the primary isoform in neurons). Studies in neuronal culture revealed that strong Zn^{2+} mobilization from these proteins in the absence of any extracellular Zn^{2+} entry, could trigger Zn^{2+} dependent neuronal injury (Aizenman et al., 2000; Bossy-Wetzel et al., 2004), and also indicated that, depending upon conditions, MT-III could either provide a source of Zn^{2+} that could injure neurons upon mobilization, or a buffer that could provide protection from cytosolic Zn^{2+} loads (Malaiyandi et al., 2004). The generation of MT-III KOs provided a model to directly examine its roles *in vivo* (Erickson et al., 1997). Interestingly, MT-III appeared to act in both of these ways, with the knockout decreasing Zn^{2+}

accumulation and injury in CA1, while increasing injury in CA3 after prolonged kainate seizure, consistent with it being a source of injurious Zn^{2+} in CA1, but buffering incoming Zn^{2+} loads to provide protection in CA3 (Erickson et al., 1997; Lee et al., 2003). Present studies extend these *in vivo* studies, by revealing distinct sources and dynamics of injurious Zn^{2+} accumulation in CA1 and CA3 neurons in acute ischemic injury, with acute entry of synaptic Zn^{2+} via Ca-AMPA channels dominating in CA3, with rapid and ongoing mobilization from MT-III appearing to dominate in CA1.

Mitochondria as critical targets of injurious Zn^{2+} effects

Whereas past studies have highlighted a number of mechanisms through which Zn^{2+} mediates neurotoxic effects, we and other have found Zn^{2+} to potently disrupt mitochondrial function *in vitro* (Weiss et al., 2000; Dineley et al., 2003; Shuttleworth and Weiss, 2011), causing dose dependent mitochondrial dysfunction that correlates well with the extent of injury evolving over the subsequent hours, leading us to hypothesize that mitochondria may be a key locus of its neurotoxic effects. Zn^{2+} appears to enter mitochondria through the MCU (Saris and Niva, 1994; Jiang et al., 2001; Malaiyandi et al., 2005; Gazaryan et al., 2007; Medvedeva and Weiss, 2014), and to affect their function with far greater potency than Ca^{2+}, causing mitochondrial depolarization, ROS generation, and potent induction of swelling, probably due to activation of a large conductance channel, the mitochondrial permeability transition pore (mPTP) (Wudarczyk et al., 1999; Jiang et al., 2001; Gazaryan et al., 2007).

Despite the high potency of its effects on isolated mitochondria, relatively high extracellular Zn^{2+} exposures are needed to potently disrupt mitochondrial function in intact neurons under resting conditions, raising questions as to the degree of mitochondrial dysfunction and injury likely to be triggered by pre-synaptic Zn^{2+} release and its translocation into post-synaptic neurons (Pivovarova et al., 2014). However, cytosolic buffering (by MT's or related peptides) is normally highly protective from cytosolic Zn^{2+} loads, and under disease associated conditions of oxidative stress and/or acidosis, buffering is impaired and mitochondrial Zn^{2+} uptake and disruption of function can occur with far lower levels, or even in the absence of extracellular Zn^{2+} (Sensi et al., 2003; Clausen et al., 2013). Indeed, intracellular

mobilization and accumulation of endogenous Zn^{2+} can impact mitochondrial function both in neuronal cultures (Sensi et al., 2003; Bossy-Wetzel et al., 2004), and in post ischemic hippocampus (Calderone et al., 2004; Bonanni et al., 2006). Furthermore, our recent slice studies strongly support the idea that specific entry of endogenous Zn^{2+} into mitochondria through the MCU contributes to ROS generation and injury during acute OGD (Medvedeva and Weiss, 2014).

Notably, mitochondria seem to be critically involved in the delayed selective degeneration of CA1 pyramidal neurons after transient ischemia; these neurons show mitochondrial swelling with release of cytochrome C into the cytosol beginning within hours of ischemia, prior to caspase-3 activation, and with the appearance of TUNEL-positive cells and neurodegeneration with prominent DNA fragmentation occurring over several days (Antonawich, 1999; Nakatsuka et al., 1999; Ouyang et al., 1999; Sugawara et al., 1999). In addition, early treatment with either the Zn^{2+} chelator, Ca-EDTA (Calderone et al., 2004) or the mPTP blocker, Cyclosporine A (CsA) (Nakatsuka et al., 1999) decreased delayed cytochrome C release in CA1 neurons after ischemia, supporting contributory roles of Zn^{2+} and the mPTP to the activation of this apoptotic pathway. In light of the potent effects of Zn^{2+} on mitochondria, we propose that the protracted Zn^{2+} accumulation we find to occur selectively in mitochondria of CA1 neurons represents a critical early and targetable event in the cascade of events culminating in the delayed selective degeneration of CA1 neurons.

Summary and therapeutic implications

Whereas *in vivo* studies have examined Zn^{2+} effects on outcome hours to days after the ischemic event, its contributions to the initiation of death cascades have been relatively little studied. Present studies employ an acute hippocampal slice model of ischemia, which provides the benefit of enabling real time high resolution tracking of changes, to assess differences in Ca^{2+} and Zn^{2+} dependent excitotoxic triggering events between CA1 and CA3 pyramidal neurons that may bear upon their differential susceptibilities. Our findings suggest that rapid "excitotoxic" Ca^{2+} and Zn^{2+} entry may dominate in CA3, possibly consistent with the particular susceptibility of these neurons after recurrent limbic seizures, which are

460 characterized by repetitive firing of Zn^{2+} rich mossy fiber terminals. However, in the case of a sublethal
461 insult, CA3 neurons may be better able to recover ionic homeostasis. In contrast to the dominant role of
462 acute Zn^{2+} translocation through Ca-AMPA channels in CA3, Zn^{2+} mobilization from MT-III appears to
463 dominate in CA1. Notably, mobilization from MT-III also appears to underlie ongoing Zn^{2+} accumulation
464 in CA1 mitochondria during the "reperfusion" phase, well after the end of sublethal episodes of OGD.
465 We suggest that this ongoing Zn^{2+} accumulation in CA1 mitochondria is integral to the delayed activation
466 of apoptotic injury in CA1, with sequential occurrence of ROS generation, mitochondrial swelling due to
467 mPTP activation, Cytochrome C release, and caspase activation contributing to delayed cell death.
468 Elucidation of these early excitotoxic events in CA1 vs CA3 pyramidal neurons may have therapeutic
469 implications. In the case of acute neuronal injury resulting from prolonged seizures or ischemia, anti-
470 excitotoxic interventions including specific block of Ca-AMPA channels may be of particular utility in
471 CA3. In contrast, while acute excitotoxic ion entry certainly contributes in CA1, interventions aiming to
472 attenuate Zn^{2+} accumulation in mitochondria (and downstream consequences thereof) may be of
473 particular value both acutely as well as after sublethal insults, to diminish delayed injury. Potential
474 interventions could include MCU blockers to attenuate delayed mitochondrial Zn^{2+} accumulation
475 (although, depending upon conditions, they also have potential to exacerbate cytosolic Ca^{2+} loading)
476 (Velasco and Tapia, 2000; Medvedeva and Weiss, 2014), antioxidants (which may attenuate oxidation
477 dependent Zn^{2+} release from MT-III), or mPTP blockers, like CsA that should attenuate downstream
478 mPTP activation (Uchino et al., 1998; Nakatsuka et al., 1999; Friberg and Wieloch, 2002). Indeed, in
479 light of the complexity of the events leading to delayed degeneration, it is likely that no single
480 intervention will be optimal, but that combinations of interventions, likely delivered in distinct temporal
481 phases of the injury cascade will provide the best outcome. We hope that further clarification of early
482 Zn^{2+} related events in CA1 vs CA3 pyramidal neurons in a model of ischemia will ultimately aid the
483 development of targeted treatments to diminish injury to these vulnerable neuronal populations after
484 ischemia or recurrent seizures.
485

References

Aizenman E, Stout AK, Hartnett KA, Dineley KE, McLaughlin B, Reynolds IJ (2000) Induction of neuronal apoptosis by thiol oxidation: putative role of intracellular zinc release. J Neurochem 75:1878-1888.

Antonawich FJ (1999) Translocation of cytochrome c following transient global ischemia in the gerbil. Neuroscience letters 274:123-126.

Assaf SY, Chung SH (1984) Release of endogenous Zn2+ from brain tissue during activity. Nature 308:734-736.

Ben-Ari Y, Tremblay E, Ottersen OP (1980a) Injections of kainic acid into the amygdaloid complex of the rat: an electrographic, clinical and histological study in relation to the pathology of epilepsy. Neuroscience 5:515-528.

Ben-Ari Y, Tremblay E, Ottersen OP, Meldrum BS (1980b) The role of epileptic activity in hippocampal and "remote" cerebral lesions induced by kainic acid. Brain Res 191:79-97.

Bonanni L, Chachar M, Jover-Mengual T, Li H, Jones A, Yokota H, Ofengeim D, Flannery RJ, Miyawaki T, Cho CH, Polster BM, Pypaert M, Hardwick JM, Sensi SL, Zukin RS, Jonas EA (2006) Zinc-dependent multi-conductance channel activity in mitochondria isolated from ischemic brain. J Neurosci 26:6851-6862.

Bossy-Wetzel E, Talantova MV, Lee WD, Scholzke MN, Harrop A, Mathews E, Gotz T, Han J, Ellisman MH, Perkins GA, Lipton SA (2004) Crosstalk between Nitric Oxide and Zinc Pathways to Neuronal Cell Death Involving Mitochondrial Dysfunction and p38-Activated K(+) Channels. Neuron 41:351-365.

Calderone A, Jover T, Mashiko T, Noh KM, Tanaka H, Bennett MV, Zukin RS (2004) Late calcium EDTA rescues hippocampal CA1 neurons from global ischemia-induced death. J Neurosci 24:9903-9913.

Choi DW (1987) Ionic dependence of glutamate neurotoxicity. The Journal of neuroscience : the official journal of the Society for Neuroscience 7:369-379.

512 Clausen A, McClanahan T, Ji SG, Weiss JH (2013) Mechanisms of Rapid Reactive Oxygen Species
513 Generation in response to Cytosolic Ca2+ or Zn2+ Loads in Cortical Neurons. Plos One
514 8:e83347.
515 Cole TB, Wenzel HJ, Kafer KE, Schwartzkroin PA, Palmiter RD (1999) Elimination of zinc from
516 synaptic vesicles in the intact mouse brain by disruption of the ZnT3 gene. Proceedings of the
517 National Academy of Sciences of the United States of America 96:1716-1721.
518 Dineley KE, Votyakova TV, Reynolds IJ (2003) Zinc inhibition of cellular energy production:
519 implications for mitochondria and neurodegeneration. J Neurochem 85:563-570.
520 Duchen MR, Surin A, Jacobson J (2003) Imaging mitochondrial function in intact cells. Methods in
521 enzymology 361:353-389.
522 Erickson JC, Hollopeter G, Thomas SA, Froelick GJ, Palmiter RD (1997) Disruption of the
523 metallothionein-III gene in mice: analysis of brain zinc, behavior, and neuron vulnerability to
524 metals, aging, and seizures. J Neurosci 17:1271-1281.
525 Frederickson CJ (1989) Neurobiology of zinc and zinc-containing neurons. Int Rev Neurobiol 31:145-
526 238.
527 Frederickson CJ, Hernandez MD, McGinty JF (1989) Translocation of zinc may contribute to seizure-
528 induced death of neurons. Brain Res 480:317-321.
529 Friberg H, Wieloch T (2002) Mitochondrial permeability transition in acute neurodegeneration.
530 Biochimie 84:241-250.
531 Gazaryan IG, Krasinskaya IP, Kristal BS, Brown AM (2007) Zinc irreversibly damages major enzymes of
532 energy production and antioxidant defense prior to mitochondrial permeability transition. J Biol
533 Chem 282:24373-24380.
534 Hollmann M, Hartley M, Heinemann S (1991) Ca2+ permeability of KA-AMPA--gated glutamate
535 receptor channels depends on subunit composition. Science 252:851-853.
536 Howell GA, Welch MG, Frederickson CJ (1984) Stimulation-induced uptake and release of zinc in
537 hippocampal slices. Nature 308:736-738.

538 Jia Y, Jeng JM, Sensi SL, Weiss JH (2002) Zn2+ currents are mediated by calcium-permeable
539 AMPA/kainate channels in cultured murine hippocampal neurones. J Physiol 543:35-48.
540 Jiang D, Sullivan PG, Sensi SL, Steward O, Weiss JH (2001) Zn(2+) induces permeability transition pore
541 opening and release of pro-apoptotic peptides from neuronal mitochondria. J Biol Chem
542 276:47524-47529.
543 Kirino T (1982) Delayed neuronal death in the gerbil hippocampus following ischemia. Brain research
544 239:57-69.
545 Koh JY, Suh SW, Gwag BJ, He YY, Hsu CY, Choi DW (1996) The role of zinc in selective neuronal
546 death after transient global cerebral ischemia. Science 272:1013-1016.
547 Koike M, Iino M, Ozawa S (1997) Blocking effect of 1-naphthyl acetyl spermine on Ca(2+)-permeable
548 AMPA receptors in cultured rat hippocampal neurons. Neuroscience research 29:27-36.
549 Lee JY, Cole TB, Palmiter RD, Koh JY (2000) Accumulation of zinc in degenerating hippocampal
550 neurons of ZnT3-null mice after seizures: evidence against synaptic vesicle origin. J Neurosci
551 20:RC79.
552 Lee JY, Kim JH, Palmiter RD, Koh JY (2003) Zinc released from metallothionein-iii may contribute to
553 hippocampal CA1 and thalamic neuronal death following acute brain injury. Exp Neurol
554 184:337-347.
555 Lerma J, Morales M, Ibarz JM, Somohano F (1994) Rectification properties and Ca2+ permeability of
556 glutamate receptor channels in hippocampal cells. The European journal of neuroscience 6:1080-
557 1088.
558 Malaiyandi LM, Dineley KE, Reynolds IJ (2004) Divergent consequences arise from metallothionein
559 overexpression in astrocytes: zinc buffering and oxidant-induced zinc release. Glia 45:346-353.
560 Malaiyandi LM, Vergun O, Dineley KE, Reynolds IJ (2005) Direct visualization of mitochondrial zinc
561 accumulation reveals uniporter-dependent and -independent transport mechanisms. J Neurochem
562 93:1242-1250.

563 Medvedeva YV, Weiss JH (2014) Intramitochondrial Zn(2+) accumulation via the Ca(2+) uniporter
564 contributes to acute ischemic neurodegeneration. Neurobiology of disease 68:137-144.
565 Medvedeva YV, Lin B, Shuttleworth CW, Weiss JH (2009) Intracellular Zn2+ accumulation contributes
566 to synaptic failure, mitochondrial depolarization, and cell death in an acute slice oxygen-glucose
567 deprivation model of ischemia. J Neurosci 29:1105-1114.
568 Moore CL (1971) Specific inhibition of mitochondrial Ca++ transport by ruthenium red. Biochemical and
569 biophysical research communications 42:298-305.
570 Nakatsuka H, Ohta S, Tanaka J, Toku K, Kumon Y, Maeda N, Sakanaka M, Sakaki S (1999) Release of
571 cytochrome c from mitochondria to cytosol in gerbil hippocampal CA1 neurons after transient
572 forebrain ischemia. Brain research 849:216-219.
573 Noh KM, Yokota H, Mashiko T, Castillo PE, Zukin RS, Bennett MV (2005) Blockade of calcium-
574 permeable AMPA receptors protects hippocampal neurons against global ischemia-induced death.
575 Proc Natl Acad Sci U S A 102:12230-12235.
576 Ogoshi F, Weiss JH (2003) Heterogeneity of Ca2+-permeable AMPA/kainate channel expression in
577 hippocampal pyramidal neurons: Fluorescence imaging and immunocytochemical assessment. J
578 Neurosci:in press.
579 Ordy JM, Wengenack TM, Bialobok P, Coleman PD, Rodier P, Baggs RB, Dunlap WP, Kates B (1993)
580 Selective vulnerability and early progression of hippocampal CA1 pyramidal cell degeneration
581 and GFAP-positive astrocyte reactivity in the rat four-vessel occlusion model of transient global
582 ischemia. Experimental neurology 119:128-139.
583 Ouyang YB, Tan Y, Comb M, Liu CL, Martone ME, Siesjo BK, Hu BR (1999) Survival- and death-
584 promoting events after transient cerebral ischemia: phosphorylation of Akt, release of cytochrome
585 C and Activation of caspase-like proteases. Journal of cerebral blood flow and metabolism :
586 official journal of the International Society of Cerebral Blood Flow and Metabolism 19:1126-
587 1135.

588 Petito CK, Feldmann E, Pulsinelli WA, Plum F (1987) Delayed hippocampal damage in humans
589 following cardiorespiratory arrest. Neurology 37:1281-1286.
590 Pivovarova NB, Stanika RI, Kazanina G, Villanueva I, Andrews SB (2014) The interactive roles of zinc
591 and calcium in mitochondrial dysfunction and neurodegeneration. J Neurochem 128:592-602.
592 Randall RD, Thayer SA (1992) Glutamate-induced calcium transient triggers delayed calcium overload
593 and neurotoxicity in rat hippocampal neurons. J Neurosci 12:1882-1895.
594 Rothman SM, Olney JW (1986) Glutamate and the pathophysiology of hypoxic--ischemic brain damage.
595 Ann Neurol 19:105-111.
596 Saris NE, Niva K (1994) Is Zn2+ transported by the mitochondrial calcium uniporter? FEBS Lett
597 356:195-198.
598 Sensi SL, Yin HZ, Weiss JH (2000) AMPA/kainate receptor-triggered Zn2+ entry into cortical neurons
599 induces mitochondrial Zn2+ uptake and persistent mitochondrial dysfunction. The European
600 journal of neuroscience 12:3813-3818.
601 Sensi SL, Ton-That D, Weiss JH (2002) Mitochondrial sequestration and Ca(2+)-dependent release of
602 cytosolic Zn(2+) loads in cortical neurons. Neurobiology of disease 10:100-108.
603 Sensi SL, Yin HZ, Carriedo SG, Rao SS, Weiss JH (1999) Preferential Zn2+ influx through Ca2+-
604 permeable AMPA/kainate channels triggers prolonged mitochondrial superoxide production. Proc
605 Natl Acad Sci U S A 96:2414-2419.
606 Sensi SL, Ton-That D, Sullivan PG, Jonas EA, Gee KR, Kaczmarek LK, Weiss JH (2003) Modulation of
607 mitochondrial function by endogenous Zn2+ pools. Proc Natl Acad Sci U S A 100:6157-6162.
608 Shuttleworth CW, Weiss JH (2011) Zinc: new clues to diverse roles in brain ischemia. Trends Pharmacol
609 Sci 32:480-486.
610 Siesjo BK (1988) Historical overview. Calcium, ischemia, and death of brain cells. Ann N Y Acad Sci
611 522:638-661.

612 Stork CJ, Li YV (2006) Intracellular zinc elevation measured with a "calcium-specific" indicator during
613 ischemia and reperfusion in rat hippocampus: a question on calcium overload. J Neurosci
614 26:10430-10437.
615 Sugawara T, Fujimura M, Morita-Fujimura Y, Kawase M, Chan PH (1999) Mitochondrial release of
616 cytochrome c corresponds to the selective vulnerability of hippocampal CA1 neurons in rats after
617 transient global cerebral ischemia. The Journal of neuroscience : the official journal of the
618 Society for Neuroscience 19:RC39.
619 Tanaka S, Kondo S, Tanaka T, Yonemasu Y (1988) Long-term observation of rats after unilateral intra-
620 amygdaloid injection of kainic acid. Brain research 463:163-167.
621 Tonder N, Johansen FF, Frederickson CJ, Zimmer J, Diemer NH (1990) Possible role of zinc in the
622 selective degeneration of dentate hilar neurons after cerebral ischemia in the adult rat. Neurosci
623 Lett 109:247-252.
624 Uchino H, Elmer E, Uchino K, Li PA, He QP, Smith ML, Siesjo BK (1998) Amelioration by cyclosporin
625 A of brain damage in transient forebrain ischemia in the rat. Brain research 812:216-226.
626 Vander Jagt TA, Connor JA, Shuttleworth CW (2008) Localized loss of Ca2+ homeostasis in neuronal
627 dendrites is a downstream consequence of metabolic compromise during extended NMDA
628 exposures. J Neurosci 28:5029-5039.
629 Velasco I, Tapia R (2000) Alterations of intracellular calcium homeostasis and mitochondrial function are
630 involved in ruthenium red neurotoxicity in primary cortical cultures. Journal of neuroscience
631 research 60:543-551.
632 Verdoorn TA, Burnashev N, Monyer H, Seeburg PH, Sakmann B (1991) Structural determinants of ion
633 flow through recombinant glutamate receptor channels. Science 252:1715-1718.
634 Wei G, Hough CJ, Li Y, Sarvey JM (2004) Characterization of extracellular accumulation of Zn2+ during
635 ischemia and reperfusion of hippocampus slices in rat. Neuroscience 125:867-877.
636 Weiss JH, Sensi SL, Koh JY (2000) Zn(2+): a novel ionic mediator of neural injury in brain disease.
637 Trends in pharmacological sciences 21:395-401.

638 Weiss JH, Hartley DM, Koh JY, Choi DW (1993) AMPA receptor activation potentiates zinc
639 neurotoxicity. Neuron 10:43-49.
640 Wudarczyk J, Debska G, Lenartowicz E (1999) Zinc as an inducer of the membrane permeability
641 transition in rat liver mitochondria. Archives of biochemistry and biophysics 363:1-8.
642 Yin HZ, Weiss JH (1995) Zn(2+) permeates Ca(2+) permeable AMPA/kainate channels and triggers
643 selective neural injury. Neuroreport 6:2553-2556.
644 Yin HZ, Sensi SL, Carriedo SG, Weiss JH (1999) Dendritic localization of Ca(2+)-permeable
645 AMPA/kainate channels in hippocampal pyramidal neurons. J Comp Neurol 409:250-260.
646 Yin HZ, Sensi SL, Ogoshi F, Weiss JH (2002) Blockade of Ca2+-permeable AMPA/kainate channels
647 decreases oxygen-glucose deprivation-induced Zn2+ accumulation and neuronal loss in
648 hippocampal pyramidal neurons. J Neurosci 22:1273-1279.
649 Zola-Morgan S, Squire LR, Amaral DG (1986) Human amnesia and the medial temporal region: enduring
650 memory impairment following a bilateral lesion limited to field CA1 of the hippocampus. The
651 Journal of neuroscience : the official journal of the Society for Neuroscience 6:2950-2967.
652
653
654
655
656

Figure Legends

Figure 1. OGD evoked Zn^{2+} rises precede and contribute to Ca^{2+} deregulation in both CA3 and CA1 pyramidal neurons. A: *Relationship between intracellular Zn^{2+} and Ca^{2+} rises, and loss of membrane integrity in individual CA3 neurons subjected to OGD.* Pseudocolor fluorescent images (**top panels**) show cells loaded with a low affinity ratiometric Ca^{2+} indicator (Fura-FF; 340/380 ratio images) along with either a Zn^{2+} sensitive indicator (FluoZin-3, background subtracted emission intensity, arbitrary units, AU; **Left**), or an ion insensitive fluorescent compound (Alexa Fluor-488, background subtracted emission intensity, AU; **Right**) and subjected to 15 min OGD. Numbers indicate time (in min) after the onset of OGD. Traces **(bottom panels)** show fluorescence changes in the same neurons. Note that the Zn^{2+} rise precedes a sharp Ca^{2+} deregulation event (**Left**), and that the Ca^{2+} deregulation is accompanied by a loss of the AlexaFluor-488 signal (**Right**, one cell representative of 4), indicative of loss of membrane integrity.

B. *Zn^{2+} rises precede the terminal Ca^{2+} deregulation in CA3 as well as CA1 pyramidal neurons:* Individual FluoZin-3 and Fura-FF loaded CA1 and CA3 neurons were subjected to OGD; traces (±SEM; aligned for the onset of Ca^{2+} deregulation) show mean changes in somatic FluoZin-3 fluorescence ($\Delta F/F_o$**; blue**) and Fura-FF ratio changes (**black**) (**CA3, Top**: Zn^{2+} rise 7.7±0.6 min, Ca^{2+} rise 11.6±0.6 min, n=8, $p=5.1x10^{-4}$; **CA1**, **Bottom**: Zn^{2+} rise 7.5±0.5 min, Ca^{2+} rise 10.6±0.5 min; n=9, $p=3.4x10^{-4}$; The interval from the Zn^{2+} rise to the Ca^{2+} deregulation was not different between CA1 and CA3; p=0.452, ANOVA linear contrast).

C. *Similar Zn^{2+} contributions to the occurrence of terminal Ca^{2+} deregulation in CA3 and CA1 pyramidal neurons:* Hippocampal slices were subjected to OGD alone (**black**) or in the presence of the Zn^{2+} chelator TPEN (40 μM; **blue**). Traces (±SEM; aligned for the onset of Ca^{2+} deregulation) show mean Fura-FF ratio changes (**CA3, Top:** control: 11.2±0.7 min, n=9; TPEN: 14.4±0.6 min, n=6, $p=5.3x10^{-3}$; **CA1, Bottom**: control: 10.6±0.5 min, n=9; TPEN: 14.7±0.7 min, n=9, $p=1.1x10^{-4}$; TPEN induced delay in Ca^{2+} deregulation was not different between CA3 and CA1, p=0.62, ANOVA linear contrast).

Figure 2. Greater contribution of acute NMDA and VGCC mediated excitotoxicity to OGD evoked Ca^{2+} deregulation in CA3 than CA1 pyramidal neurons. CA1 and CA3 neurons were loaded with FluoZin-3 and Fura-FF, and subjected to OGD alone (**black**), in the presence of the NMDA receptor antagonist, MK-801 (**MK**, **red**; 10 μM) or with both MK-801 and the VGCC blocker nimodipine (**MK/Nim**, **blue**; both at 10 μM); traces (±SEM; aligned for the onset of Ca^{2+} deregulation) show mean Fura-FF ratio changes. Each of these anti-excitotoxic interventions delays Ca^{2+} deregulation in both CA3 **(A)** and in CA1 **(B) (CA3:** control: 11.1±0.6, n=13; MK-801: 17.5±0.5, n=5, $p=5.7x10^{-6}$; MK/Nim: 20.2±0.9 min, n=10, $p=7.8x10^{-9}$ vs control for both treatments; **CA1:** control: 10.6±0.5 min, n=9; MK-801: 13.5±1.1 min, n=7, p=0.017; MK/Nim:16.7±0.8 min, n=10, $p=1.4x10^{-5}$ vs control. Notably, each of these interventions provides a greater degree of protection in CA3 than in CA1 (p=0.044 for MK801 alone and p=0.019 for MK/Nim by ANOVA linear contrast).

Figure 3. Contribution of synaptic Zn^{2+} release and its entry through Ca-AMPA channels to OGD evoked Ca^{2+} deregulation in CA3 pyramidal neurons. CA1 and CA3 neurons in slices from wild type mice (**A**) and ZnT3 KO mice (**B**) were loaded with Fura-FF and FluoZin-3 and subjected to OGD alone (**black**) or in the presence of TPEN (40 μM) or NASPM (100 μM) as indicated (**blue**). Traces (±SEM; aligned for the onset of Ca^{2+} deregulation) show mean Fura-FF ratio changes.

A. *Ca-AMPA channel blockade substantially delays Ca^{2+} deregulation in CA3 (**Left**), with no effect on CA1 neurons (**Right**).* (**CA3:** control: 11.5±0.7 min, n=7; NASPM: 18.1±1.2 min, n=5; $p=6x10^{-4}$**; CA1:** control: 10.6±0.5 min, n=9; NASPM: 10.7±0.4 min, n=5; p=0.86)

B. *In the absence of vesicular Zn^{2+} (in ZnT3 KO's), protective effects of TPEN and of NASPM on CA3 neurons are eliminated (but TPEN still protects in CA1).* (**CA3:** control: 12.1±0.9 min, n=9; NASPM: 12.8±0.9 min, n=9, p=0.58; TPEN: 12.2±0.6 min, n=6, p=0.96; **CA1**: control: 8.4±0.8 min, n=6; TPEN: 11.5±1.0 min, n=7**,** p=0.037)

Figure 4: MT-III deletion substantially eliminates the Zn^{2+} contribution to acute OGD induced injury in CA1 (but not CA3) pyramidal neurons. CA1 and CA3 neurons in slices from MT-III KO mice were loaded with Fura-FF and FluoZin-3 and subjected to OGD alone (**black**), or in the presence either of TPEN (40 μM) or MK-801+ nimodipine (MK/Nim, each at 10 μM) as indicated (**blue**). Traces (±SEM; aligned for the onset of Ca^{2+} deregulation) show mean Fura-FF ratio changes.

A. *In the absence of MT-III, protective effects of TPEN persist in CA3* ***(Left)*** *but are eliminated in CA1* ***(Right)***. (**CA3:** control: 10.2±0.7 min, n=8, TPEN: 13.6±0.7 min, n=8, $p=3.7x10^{-3}$; **CA1:** control: 11.6±0.7 min, n=9, TPEN: 12.0±0.8 min, n=7, p=0.76)

B. *In the absence of MT-III, NMDA and VGCC mediated excitotoxicity contributes substantially to OGD evoked Ca^{2+} deregulation in both CA3 and CA1 pyramidal neurons.* (**CA3:** control: 10.2±0.7 min, n=8, MK/Nim: 17.2±1.2 min, n=7, $p=5.2x10^{-4}$; **CA1:** control: 13.0±0.7 min, n=9, MK/Nim: 20.4±0.7 min, n=10, $p= 3.1x10^{-7}$; MK/Nim induced delay in Ca^{2+} deregulation was not different between CA3 and CA1, p=0.78, ANOVA linear contrast)

Figure 5. Sublethal OGD evokes delayed mitochondrial Zn^{2+} accumulation in CA1 but not in CA3 pyramidal neurons. A,B,C: Individual CA1 and CA3 neurons in slices from wild type mice were loaded with Fura-FF and FluoZin-3, subjected to sublethal episodes of OGD (~7-10 min, OGD terminated **~1 min** after the initial cytosolic Zn^{2+} rise), and cytosolic Zn^{2+} (monitored as FluoZin-3 $\Delta F/F_o$) followed for an additional hour (**A:** without; or **B,C:** with delayed addition of FCCP, 2μM x 5 min, as indicated). Pseudocolor images show FluoZin-3 fluorescence in single representative neurons at the indicated times after the start of OGD (in min), and traces (FluoZin-3 $\Delta F/F_o$**; blue**; Fura-FF ratio; **black**) show time course of changes in the same neurons (mean start times of the initial OGD-evoked Zn^{2+} rise were: **A:** 8.0±0.8 min, n=5; **B:** 7.7±0.75 min, n=7; **C:** 7.2±0.38 min, n=8 neurons).

A. *Cytosolic Zn^{2+} rise and slow recovery in CA1 neurons after sublethal OGD*. Note the further rise after the termination of OGD followed by a slow recovery of cytosolic Zn^{2+} over the ~30 min after the OGD (trace representative of n=5).

B,C. *Administration of FCCP 55-60 min after OGD termination evoked large cytosolic Zn^{2+} rises in CA1 but not in CA3 neurons.* (Mean FCCP elicited Zn^{2+} rises at 55-60 min: **CA1**: 75±21.9%, n=7; **CA3**: 8.75±7.4%, n=8, $p=3.5x10^{-3}$)

D,E. *Substantial recovery of mitochondrial potential ($\Delta\Psi_m$) in both CA1 and CA3 pyramidal neurons after sublethal OGD.* Slices were bath loaded with Rhod123 and subjected to sublethal (9 min) OGD followed after ~50 min by FCCP application as indicated. Traces (from representative single neurons) demonstrate changes in Rhod123 fluorescence relative to the pre-OGD baseline (ΔF_{OGD}). However, since slow dye loss from the slices after OGD attenuated absolute ΔF rises, for quantitative comparisons of magnitudes of ΔF changes (reflecting the degree of ΔΨm loss triggered by OGD vs that triggered by FCCP) responses were re-normalized to the 3 min just prior to addition of FCCP ($\Delta F_{\mathbf{FCCP}}$; red) (**CA1**: $\Delta F_{\mathbf{OGD}}$ 63±5.7%, $\Delta F_{\mathbf{FCCP}}$ 58.7±5.2%, $\Delta F_{FCCP}/\Delta F_{OGD}$ 0.98±0.14, n=6; **CA3**: $\Delta F_{\mathbf{OGD}}$ 56±3.5%, $\Delta F_{\mathbf{FCCP}}$ 56±10%, $\Delta F_{FCCP}/\Delta F_{OGD}$1.02±0.19, n=7; p=0.88).

Figure 6. Delayed mitochondrial Zn^{2+} uptake in CA1 pyramidal neurons is substantially attenuated by MCU inhibition shortly after OGD or by deletion of MT-III. CA1 neurons were co-loaded with FluoZin-3 and Fura-FF and subjected to sublethal OGD, followed, after 55-60 (A,C) or ~70 (B) min, by addition of FCCP (2μM x 5 min). Traces show the time course of changes in FluoZin-3 $\Delta F/F_o$ (**blue**) and Fura-FF ratio (**black**) in representative neurons (mean start times of the initial OGD-evoked Zn^{2+} rise were: **A:** 7.6±0.6 min, n=7; **B:** 7.0±0.4 min, n=6; **C:** 7.1±0.3 min, n=10).

A,B. *MCU inhibition only blocks mitochondrial Zn^{2+} uptake when applied shortly after OGD, while cytosolic Zn^{2+} is elevated:* RR (10 μM for 15 min) was applied ~7-10 min (**A**) or ~35-40 min (**B**) after OGD (traces show representative single neurons), followed by application of FCCP as indicated. Note the absence of FCCP elicited Zn^{2+} rise with early application of RR while cytosolic Zn^{2+} was still elevated (**A**), in contrast to the strong FCCP elicited Zn^{2+} rise with later application of RR (**B**). Also note the small intracellular Zn^{2+} rise triggered by late RR application, most likely resulting from block of ongoing Zn^{2+} uptake into mitochondria at this late time point (**Arrow**, seen in 6 of 6 cells examined). (Mean FCCP

elicited Zn^{2+} rises, as FluoZin-3 $\Delta F/F_o$: **A:** 6.3±4.2%, n=7, $p=1.7x10^{-3}$; **B:** 68±18.3%, n=6, p=0.8; *both comparisons with the rise in control, 75±21.9%, from Fig. 5B*).

C. *Diminished delayed mitochondrial Zn^{2+} accumulation in CA1 pyramidal neurons of MT-III KO mice*. Hippocampal neurons from MT3 mice were loaded with indicators and subjected to sublethal OGD followed by application of FCCP as in Fig. 5B. Note the paucity of Zn^{2+} rise triggered by FCCP exposure compared to that seen in WT mice (FluoZin-3 $\Delta F/F_o$: 20.7±8%, n=10).

D. *Summary data: Delayed mitochondrial Zn^{2+} uptake as a function of treatment.* Bars indicate mean FCCP evoked Zn^{2+} rises (normalized to the pre-FCCP baseline, ΔF_{FCCP}) after sublethal OGD under the conditions indicated. ***** indicates $p<0.01$ vs CA1 control; (p values vs CA1 control are as indicated above: CA1 early RR: $p=1.7x10^{-3}$; CA1 late RR: p=0.8; CA3: $p=3.5x10^{-3}$; #, for CA1 MT-III KO we elect not to display a p value because of strain difference).

Figure 7. Mitochondrial swelling after OGD in CA1 pyramidal neurons is attenuated by MCU blockade. Brain slices were subjected to sham wash in oxygenated medium (control) or were subjected to 8.5 min OGD either alone or with RR (10 μM, applied 10 min after termination of the OGD for 15 min). One hour after the end of the OGD, slices were fixed (with 4% PFA), and processed for immunostaining with TOM20 antibody.

A. *Appearance of mitochondrial swelling.* Representative merged images show the brightfield appearance of pyramidal neurons in the CA1 region overlaid with confocal fluorescence images of TOM-20 labeled mitochondria. Bar =10μm

B. *Quantitative measurements.* **Left:** Mitochondrial measurements (length and width; obtained using ImageJ software, see Methods) after the indicated treatment. **G**raphs display mean values from 3-5 independently treated hippocampal slices, comprising ≥ 18 neurons each condition, and with 107 mitochondria measured in control; 144 in OGD; 190 in OGD+RR (see Methods; *Length, in μm: control 1.4±0.047, OGD 0.8±0.032, $p=2.0x10^{-4}$ vs control; OGD+RR 1.0±0.062, $p=8x10^{-3}$ vs control, p=0.04 vs*

OGD; Width: control 0.49±0.007, OGD 0.64±0.045, p=0.03 vs control; OGD+RR 5.5±0.024, p=0.09 vs control, p=0.1 vs OGD). **Right:** Mean Length/Width (**L/W**) ratios observed after each treatment *(based on the same data; control 2.9±0.1, OGD 1.4±0.11, $p=1.9x10^{-4}$ vs control; OGD+RR 2.0±0.17, $p=7.9x10^{-3}$ vs control, p=0.03 vs OGD*). Note that OGD caused a "rounding up" of mitochondria, with a decrease in length and increase in width; and that this change was attenuated by delayed treatment with RR. * - P<0.05, ** - P<0.01, *** - P<0.001

Figure 8: Schematic model: Possible acute and early "reperfusion" events after sublethal ischemia in CA1 pyramidal neurons. Traces show representative FluoZin-3 changes from a single neuron and Rhod123 changes from the CA1 pyramidal cell layer of a different slice. **(1) Early OGD:** Zn^{2+} (circles) and glutamate (triangles) are released from presynaptic terminals. Zn^{2+} and Ca^{2+} enter post-synaptic neurons via glutamate activated (Ca-AMPA & NMDA) channels and VGCC. Zn^{2+} is also mobilized from MT-III as a result of ischemia associated oxidative stress and acidosis. Intracellular Zn^{2+} and Ca^{2+} are taken up by mitochondria (via the MCU). Mitochondrial dysfunction including ROS generation, will promote further Zn^{2+} mobilization, resulting in a feed forward cascade of mitochondrial dysfunction and Zn^{2+} accumulation. This uptake causes early mitochondrial depolarization (loss of $\Delta\Psi_m$) which precedes the sharp cytosolic Zn^{2+} rise. **(2): Later during OGD:** After some threshold of mitochondrial Zn^{2+} and Ca^{2+} accumulation, mitochondria strongly depolarize (loss of $\Delta\Psi_m$) and the Zn^{2+} and Ca^{2+} sequestered within them are released back into the cytosol. At this point, the oxidative and acidotic environment combined with mitochondrial dysfunction will impair both the buffering of Zn^{2+} by MT-III, and cellular extrusion of Ca^{2+} and Zn^{2+}, impeding recovery of ionic homeostasis. In the absence of prompt reperfusion, severe cytosolic Ca^{2+} deregulation and rapid cell death ensues. **(3) "Reperfusion" after sublethal OGD:** If reperfusion with restoration of O_2 and glucose occurs prior to the onset of Ca^{2+} deregulation, mitochondria can begin to recover function and $\Delta\Psi_m$. With recovery of $\Delta\Psi_m$ (along with oxidative environment possibly worsened by reperfusion), cytosolic Zn^{2+} is taken back up into mitochondria, where it can remain sequestered for extended periods of time [likely hours; (Sensi et al.,

2002; Bonanni et al., 2006)], and can impair their function [likely synergistically with Ca^{2+}; (Sensi et al., 2000; Jiang et al., 2001)]. Depending upon the extent of Zn^{2+} uptake, mitochondria might gradually recover their normal function, or, alternatively, may undergo delayed dysfunction, comprising ROS production and opening of the mPTP [with release of cytochrome C (CyC) and other apoptotic mediators], contributing to delayed cell death. Such a mechanism is compatible with findings of preferential delayed mitochondrial dysfunction with CyC release in CA1 pyramidal neurons after transient ischemia (Nakatsuka et al., 1999; Sugawara et al., 1999).

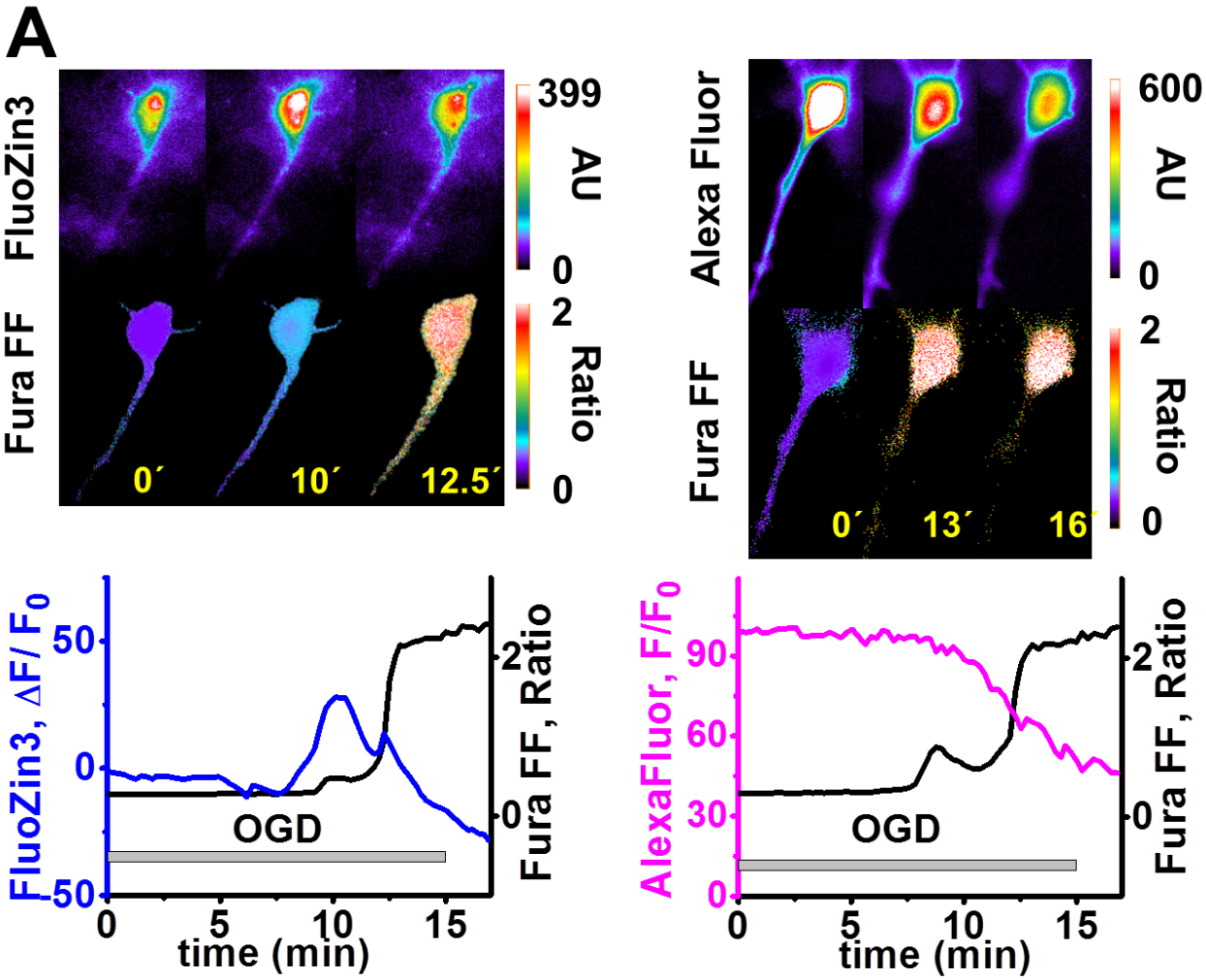
A
FluoZin3
Fura FF
399
AU
0
2
Ratio
0
0´
10´
12.5´
Alexa Fluor
600
AU
0
2
Ratio
0
0´
13´
16´
FluoZin3, ΔF/ F0
50
0
-50
Fura FF, Ratio
2
0
OGD
0
5
10
15
time (min)
AlexaFluor, F/F0
90
60
30
0
Fura FF, Ratio
2
0
OGD
0
5
10
15
time (min)

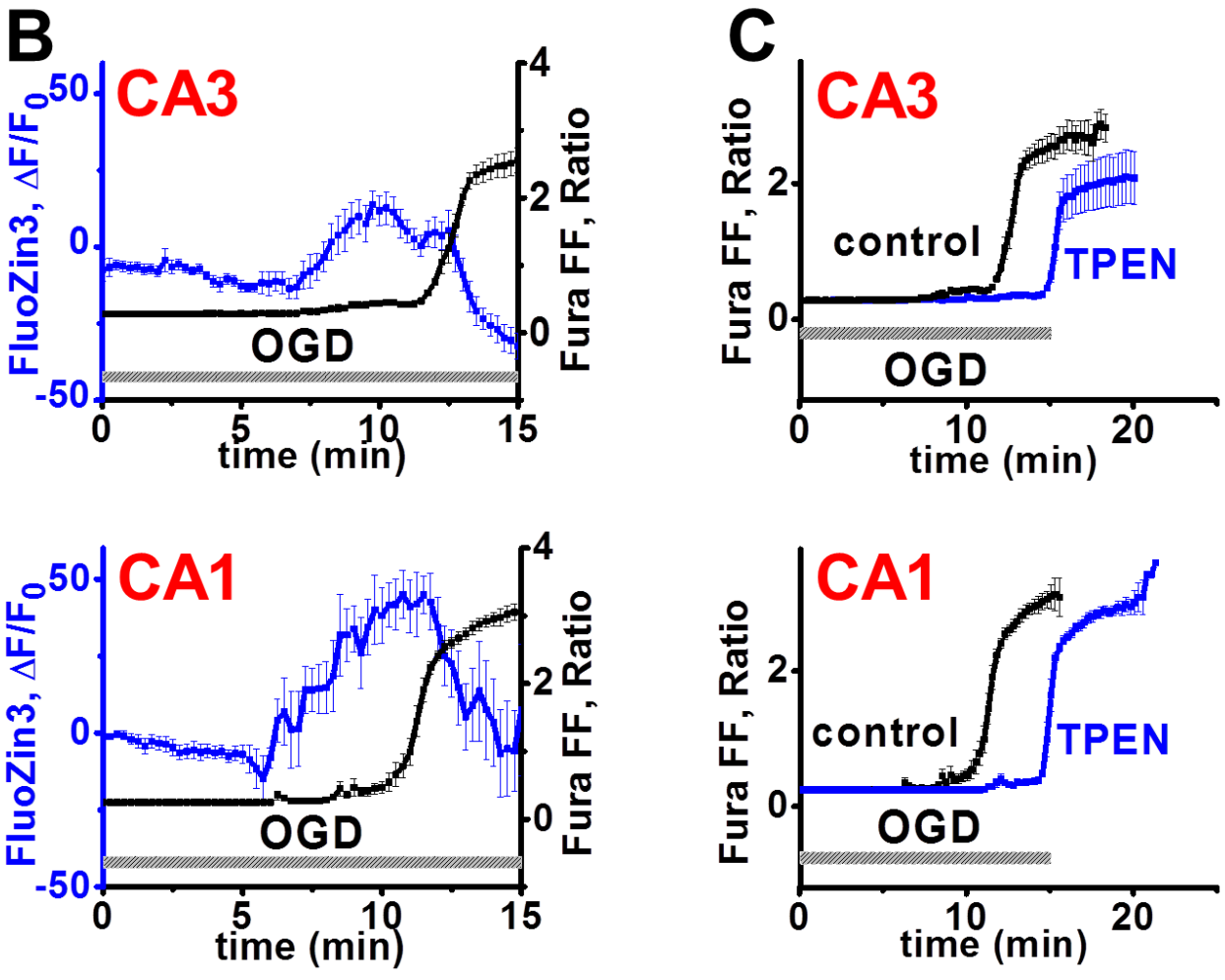
B
CA3
FluoZin3, ΔF/F0
50
0
-50
Fura FF, Ratio
4
2
0
OGD
0
5
10
15
time (min)
CA1
FluoZin3, ΔF/F0
50
0
-50
Fura FF, Ratio
4
2
0
OGD
0
5
10
15
time (min)
C
CA3
Fura FF, Ratio
2
0
control
TPEN
OGD
0
10
20
time (min)
CA1
Fura FF, Ratio
2
0
control
TPEN
OGD
0
10
20
time (min)

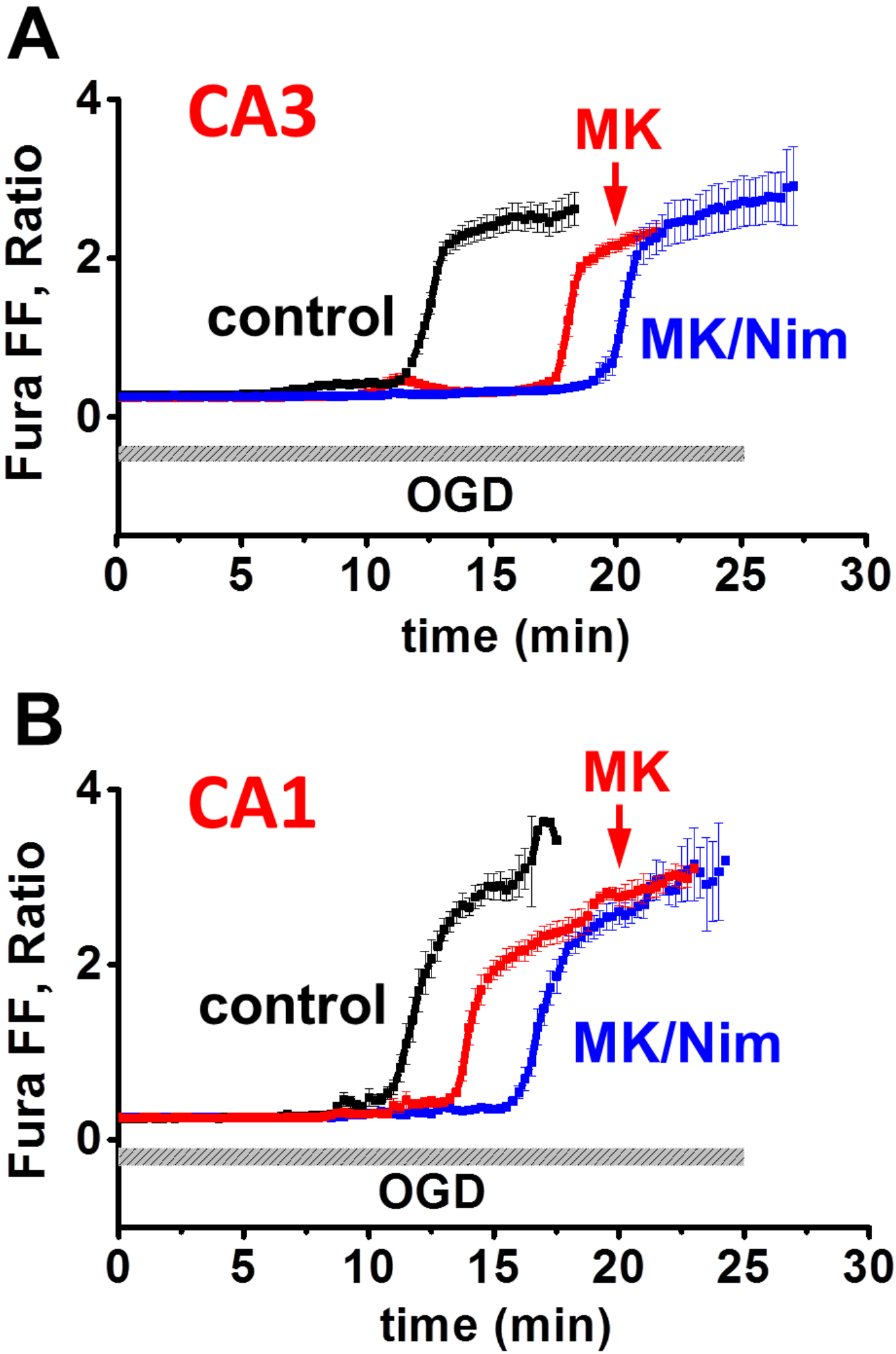
A
CA3
MK
control
MK/Nim
OGD
Fura FF, Ratio
time (min)
B
CA1
MK
control
MK/Nim
OGD
Fura FF, Ratio
time (min)

A. WT mice

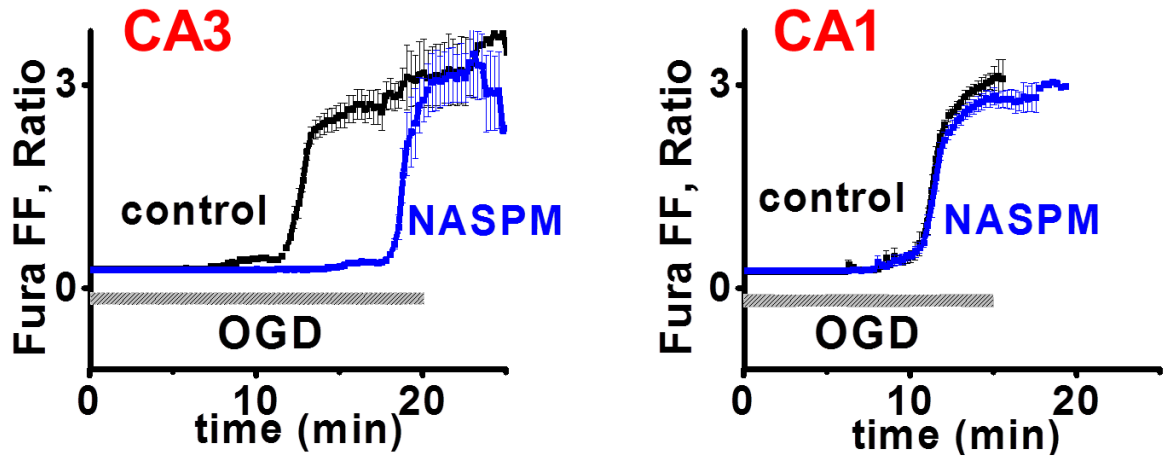

B. ZnT3 KO mice

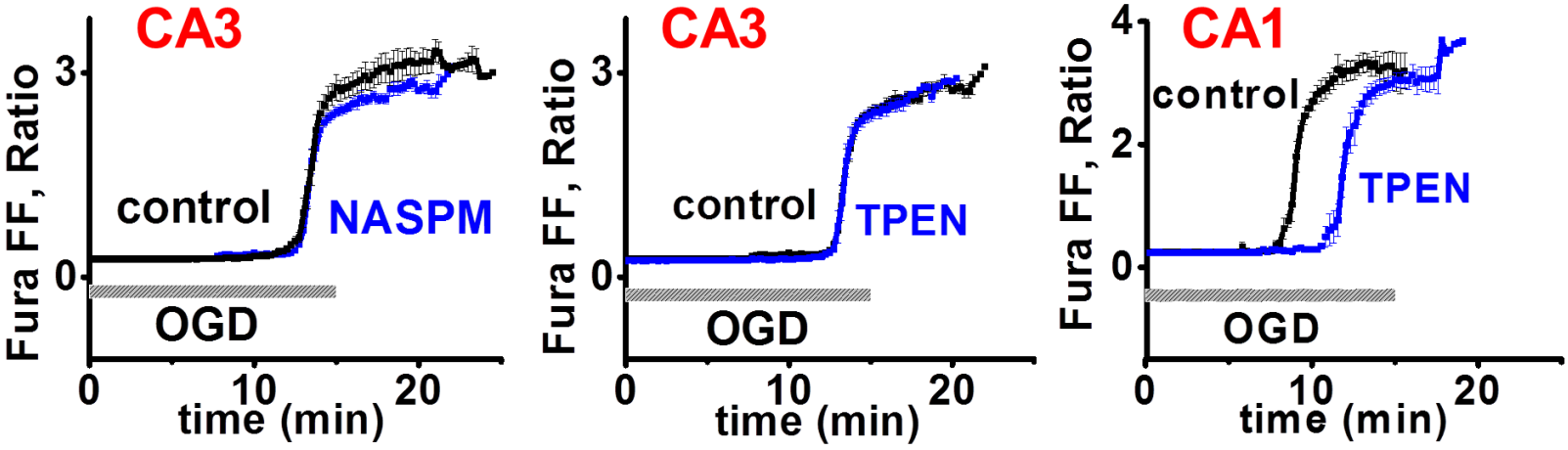

MT-III KO mice

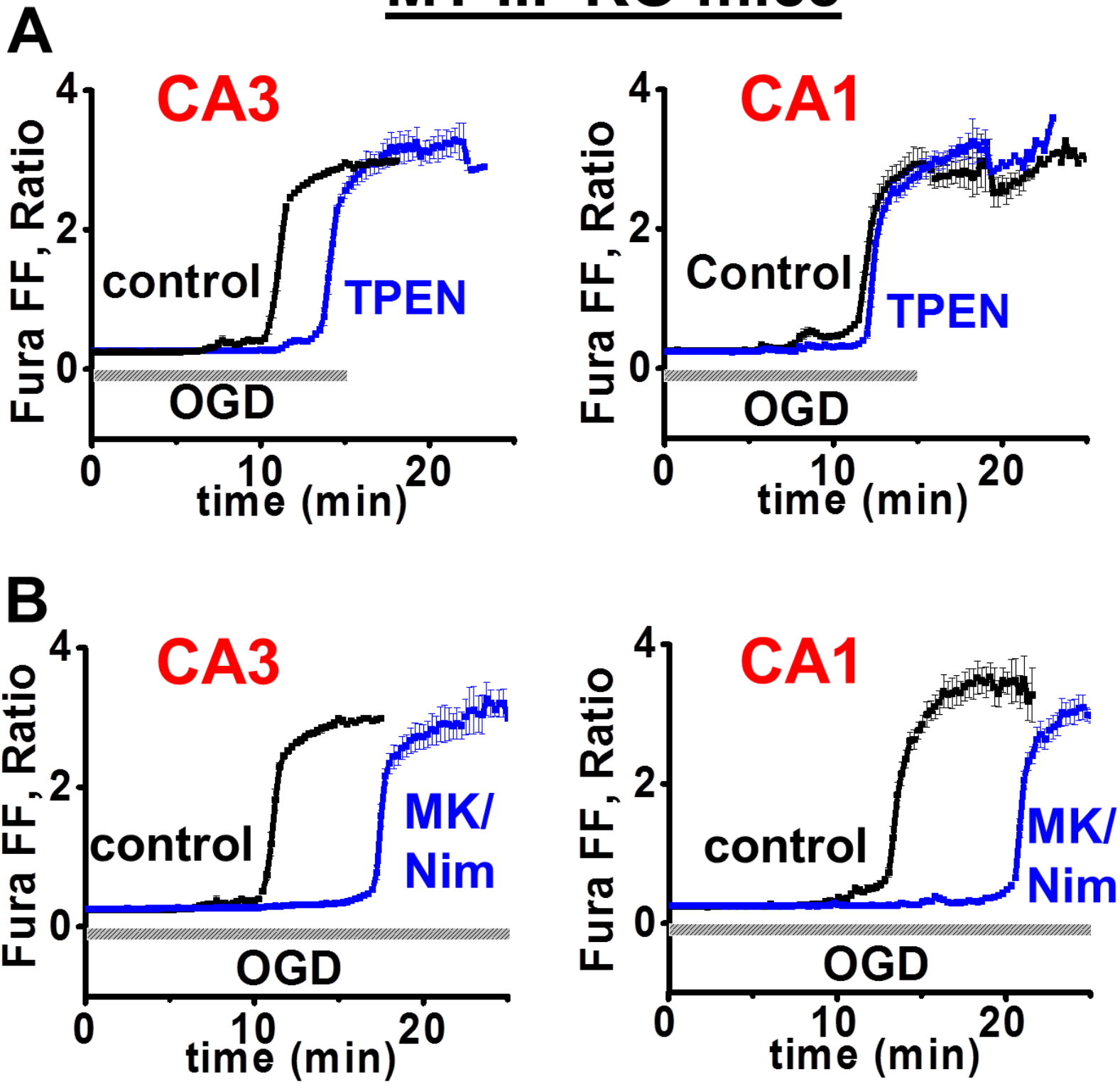

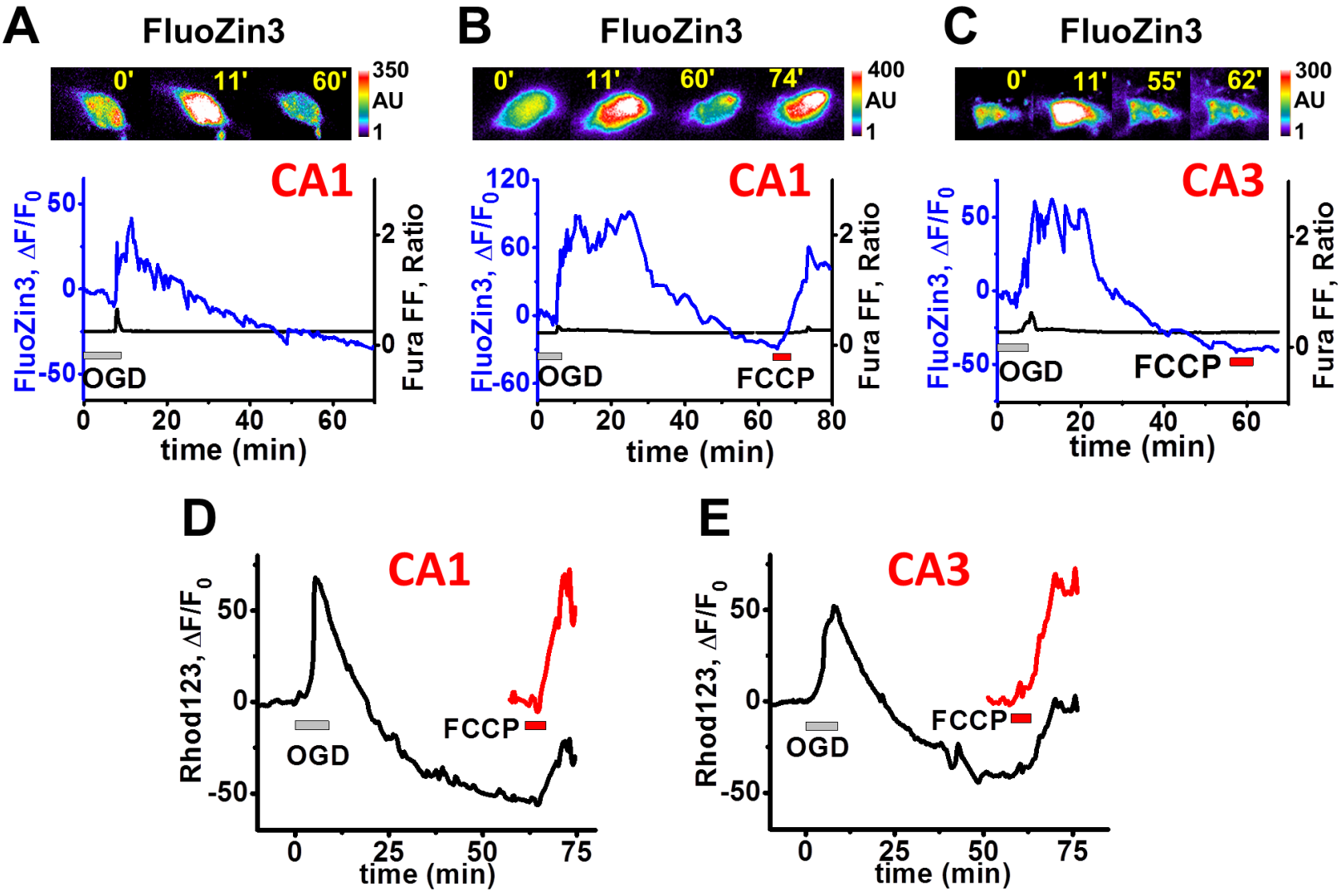
A
FluoZin3
0'
11'
60'
350
AU
1
CA1
FluoZin3, ΔF/F0
Fura FF, Ratio
OGD
time (min)
B
FluoZin3
0'
11'
60'
74'
400
AU
1
CA1
FCCP
C
FluoZin3
0'
11'
55'
62'
300
AU
1
CA3
D
CA1
Rhod123, ΔF/F0
E
CA3

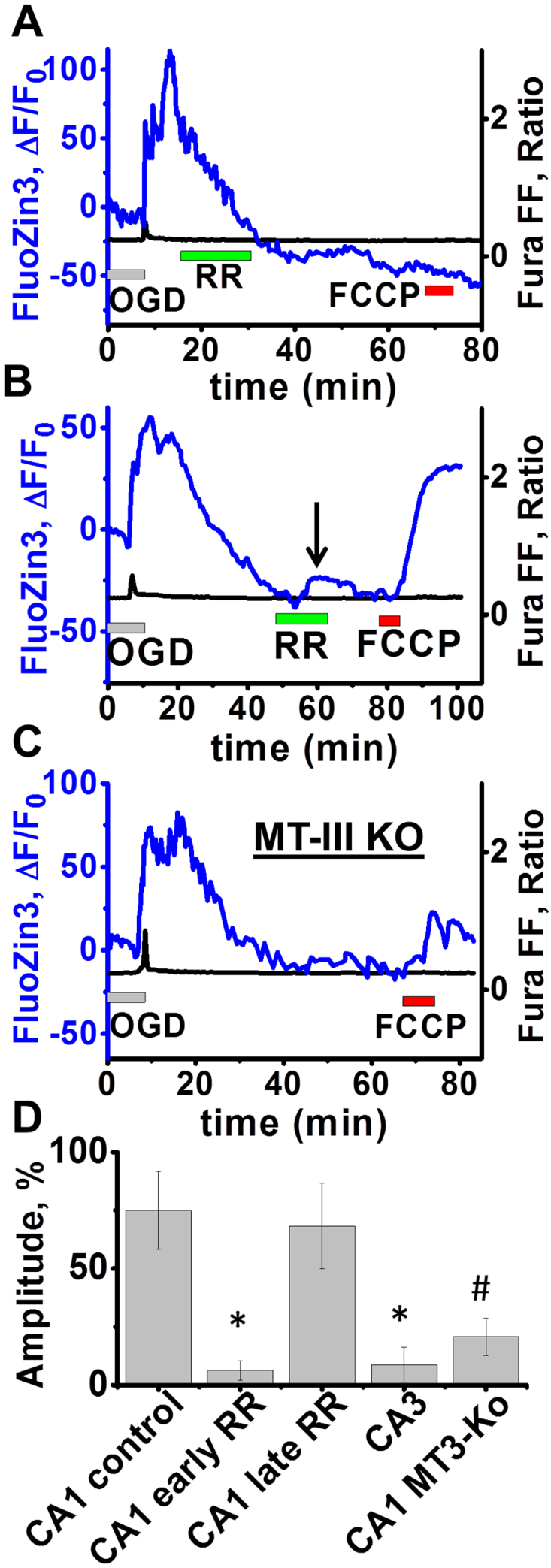
A
FluoZin3, ΔF/F0
Fura FF, Ratio
OGD
RR
FCCP
time (min)
B
FluoZin3, ΔF/F0
Fura FF, Ratio
OGD
RR
FCCP
time (min)
C
MT-III KO
FluoZin3, ΔF/F0
Fura FF, Ratio
OGD
FCCP
time (min)
D
Amplitude, %
CA1 control
CA1 early RR
CA1 late RR
CA3
CA1 MT3-Ko

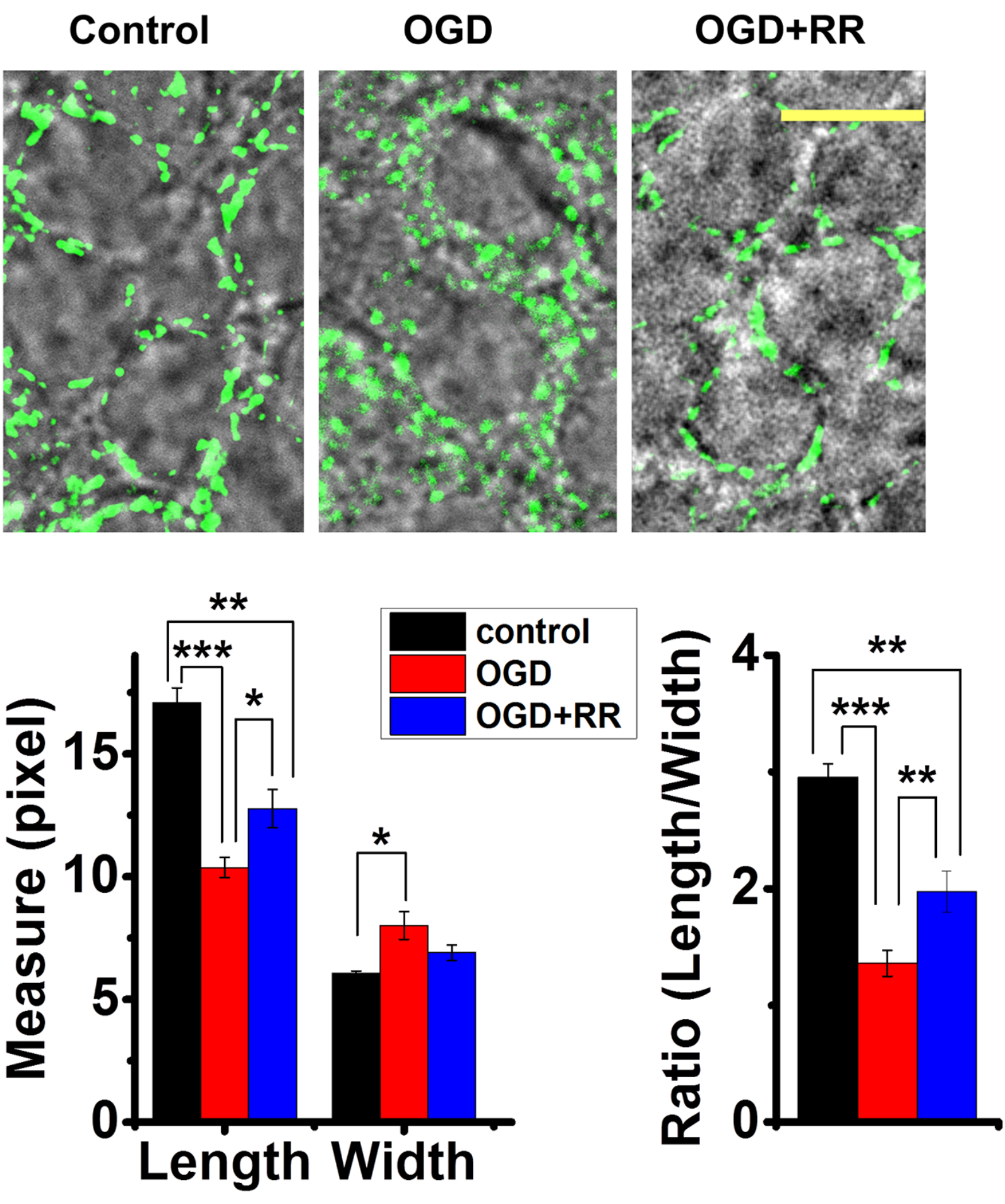
Control
OGD
OGD+RR
control
OGD
OGD+RR
Measure (pixel)
0
5
10
15
**
***
*
*
Length
Width
Ratio (Length/Width)
0
2
4
**
***
**

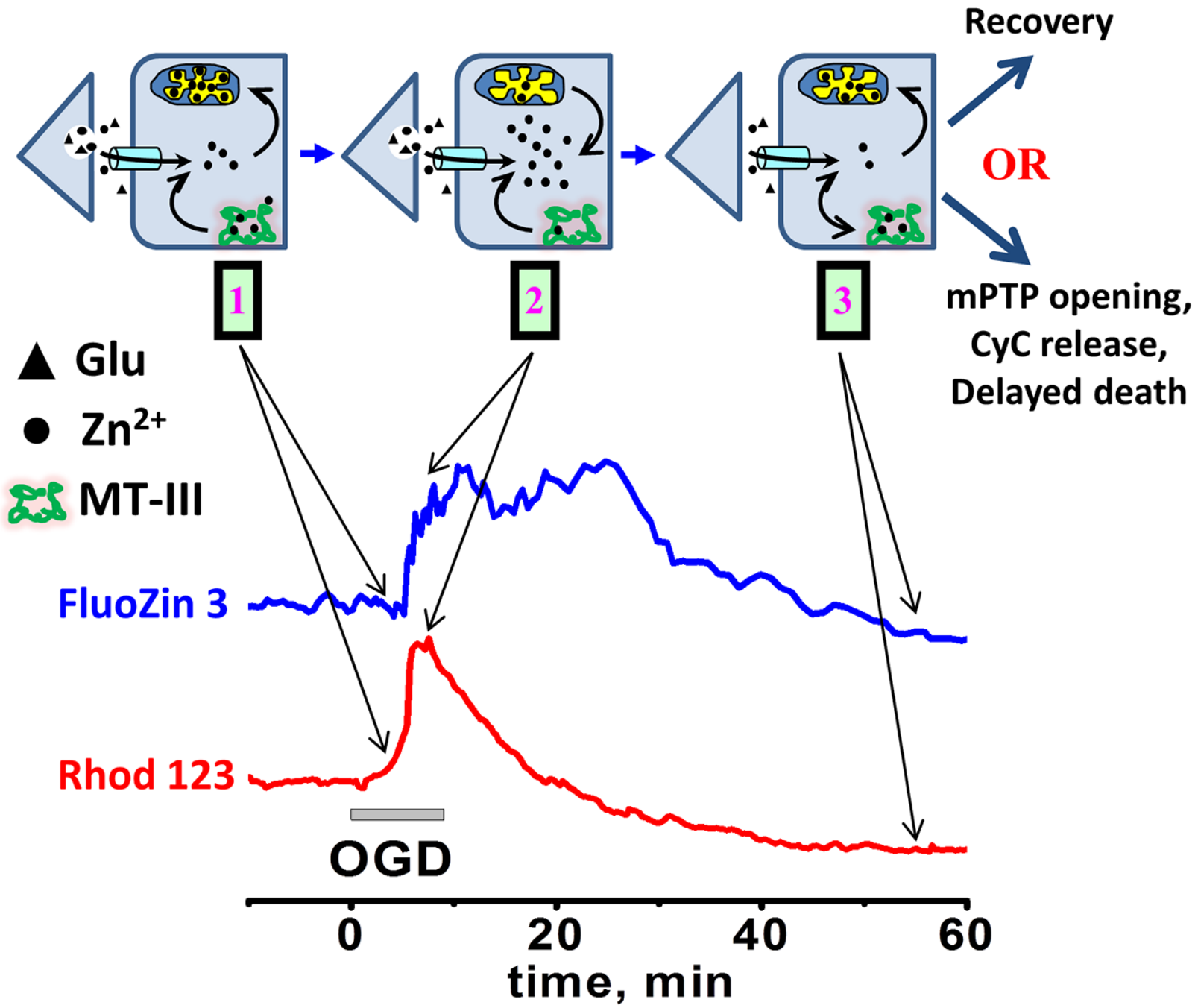
Recovery
OR
mPTP opening,
CyC release,
Delayed death
1
2
3
Glu
Zn^{2+}
MT-III
FluoZin 3
Rhod 123
OGD
0
20
40
60
time, min